ELSEVIER

Biochimica et Biophysica Acta 1412 (1999) 149–172

BIOCHIMICA ET BIOPHYSICA ACTA

BBA

www.elsevier.com/locate/bba

Uphill energy transfer in LH2-containing purple bacteria at room temperature

Hans-Wilhelm Trissl [a,*], Christopher J. Law [b], Richard J. Cogdell [b]

[a] *Abteilung Biophysik, University of Osnabrück, Fachbereich Biologie/Chemie, Barbarastrasse 11, D-49069 Osnabrück, Germany*

[b] *Division of Biochemistry and Molecular Biology, University of Glasgow, Glasgow G12 8QQ, UK*

Received 15 February 1999; received in revised form 7 April 1999; accepted 3 May 1999

Abstract

Uphill energy transfer in the LH2-containing purple bacteria *Rhodopseudomonas acidophila*, *Rhodopseudomonas palustris*, *Rhodobacter sphaeroides*, *Chromatium vinosum* and *Chromatium purpuratum* was studied by stationary fluorescence spectroscopy at room temperature upon selective excitation of the B800 pigments of LH2 and the B880 pigments of LH1 at 803 nm and 900 nm, respectively. The resulting fluorescence spectra differed significantly at wavelengths shorter than the fluorescence maximum but agreed at longer wavelengths. The absorption spectra of the species studied were decomposed into five bands at approx. 800, 820, 830, 850 and 880 nm using the shapes of the absorption spectra of the LH1-RC only species *Rhodospirillum rubrum* and the isolated B800-850 complex from *Rps. acidophila* strain 10050 as guide spectra. This allowed a quantification of the number of pigments in each pigment group and, consequently, the antenna size of the photosynthetic unit assuming 36 bacteriochlorophyll *a* molecules in an LH1-RC complex. In most of the LH2-containing purple bacterial strains the number of LH2 rings per LH1-RC was less than the idealized number of eight (Papiz et al., Trends Plant Sci. 1 (1996) 198–206), which was achieved only by *C. purpuratum*. Uphill energy transfer was assayed by comparing the theoretical fluorescence spectrum obtained from a Boltzmann equilibrium with the measured fluorescence spectrum obtained by 900 nm excitation. The good match of both spectra in all the purple bacteria studied indicates that uphill energy transfer occurs practically up to its thermodynamically maximal possible extent. All strains studied contained a small fraction of either poorly connected or unconnected LH2 complexes as indicated by higher fluorescence yields from the peripheral complexes than predicted by thermal equilibration or kinetic modeling. This impedes generally the quantitative analysis of blue-excited fluorescence spectra.

Keywords: Purple bacterium; Fluorescence yield; Peripheral light harvesting complex; LH2; Antenna size

1. Introduction

The photosynthetic apparatus of phototrophic organisms consists of a so-called 'core' complex which is intimately associated with the photochemical reaction center (RC) and, in many cases, peripheral light harvesting (LH) complexes. Usually these peripheral complexes are comprised of antenna pigments that are blue-shifted compared to those of the core complexes. The absorption of light energy by the peripheral antenna system creates excited states that then proceed energetically 'downhill', from the peripheral to the core complexes. However, in the cyanobacterium *Synechococcus* (formerly *Anacystis nidulans*) [1,2], red alga *Porphyridium cruentum* [2], plant pho-

* Corresponding author. Fax: +49 (541) 9692870.

0005-2728/99/$ – see front matter
PII: S0005-2728(99)00056-0

tosystem (PS) II [3] and the purple bacterium *Rhodobacter* (*Rb.*) *sphaeroides* [4] it was shown that the reverse back-transfer or 'uphill' process is also possible. To date, the extent of this uphill transfer process in the purple bacteria has not been studied extensively and is open to debate.

The purple bacteria possess spectrally well defined pools of bacteriochlorophyll (BChl) *a* or *b* antenna pigments. These pigments are densely packed in circularly degenerate rings [5] in which equilibration is reached within less than 1 ps [6]. The different pools of BChl are designated according to their NIR absorption bands which are located near 800 nm (B800), 820 nm (B820), 850 nm (B850), and 880 nm (B880). These terms are used generically here irrespective of the exact location of the absorption maximum. When present, the B800 and B820 (or B800 and B850) BChls are non-covalently bound to aggregates of eight or nine α,β-polypeptide dimers [7,8] that form the peripheral LH2 ring complexes. These complexes surround, in a variable stoichiometric ratio [9], the core LH1 ring complex which is composed of 16 B880-binding α,β-polypeptide dimers [10]. The 'hole' in the center of the LH1 ring accommodates the RC. Based on molecular modeling techniques, Papiz et al. [5] have suggested that optimal packing of the photosynthetic unit (PSU) occurs when the core complex is surrounded by eight LH2 rings. However, little experimental data exist on the actual in vivo stoichiometries.

Thermal equilibration has been implicated by van Grondelle [11] to hold for purple bacterial light-harvesting systems. Indeed, a picosecond equilibration amongst all LH1 and LH2 antenna pigments was shown by time-resolved fluorescence decay measurements of *Rhodobacter capsulatus* [12]. Other researchers have reported equilibration times ranging from between 20 and 35 ps [13] to between 35 and 50 ps [14]. However, uncertainty still remains as to whether or not the idealized case of thermal equilibration is an appropriate approximation for heterogeneous LH2-LH1 antenna systems. Consider the simplest case in which the excited state can distribute between two chromophores (or pigment pools), A and B, each having a kinetically distinct decay channel $\leftarrow A \leftrightarrow B \rightarrow$. In this scenario, excitation of either A or B leads to an unbalanced state which subsequently may pass into a transfer equilibrium depending on the rate constants involved. This transfer equilibrium may be close to the thermal equilibrium, again depending on the rate constants involved. In the case of PS I and PS II it has been shown that the transfer equilibrium may differ substantially from the Boltzmann distribution, i.e. thermal equilibrium [15]. This may also be the case in the purple bacterial photosynthetic system. However, a complete analysis of such systems must also take into account the kinetics prior to the establishment of the transfer equilibrium.

In purple bacteria sequential downhill energy transfer from B800 to B880 occurs via B850 (or B820/830). The B800 to B850 transfer is extremely rapid, occurring within 0.7 ps [16–22] and, therefore, fluorescence from the B800 pigments is negligibly small [23]. For the next energy transfer step ($B850 \rightarrow B880$) rather diverging times ranging from 2 to 40 ps and even some biphasic kinetics have been reported [7,14,16,24–26]. The deactivation rate constant of B880 with open RCs, i.e. the trapping time, is of a similar order with $k_t \approx (60\ \text{ps})^{-1}$ [27–32]. When the RCs are closed (P^+) this trapping time increases approx. 3-fold [11]. The back reaction rate constants are then related to the forward rate constants by a combination of the Boltzmann factor and the entropy term (Eq. 7 in [11]). Therefore, depending upon the upper or lower limit of the $B850 \rightarrow B880$ transfer step, one would expect fluorescence emission spectra that deviate, to a greater or lesser extent, from thermal equilibrium spectra. In particular, markedly different spectra would be expected at an excitation wavelength of 800 nm (downhill transfer) compared to one of 880 nm (uphill transfer). This provides a useful assay for studying the energy transfer dynamics in different purple bacteria. It is important to note that the maximal extent of uphill transfer is given by the thermal equilibrium [11,33].

To assess whether or not any generalized conclusions can be drawn about the extent of uphill energy transfer towards equilibration we studied, by stationary fluorescence measurements, several species of LH2-LH1 containing purple bacteria. In addition we attempted a spectral decomposition of the LH2+LH1-RC systems, based on the assumption of invariant oscillator strengths in the different pigment pools.

2. Materials and methods

2.1. Chromatophore preparation

Rhodopseudomonas (*Rps.*) *acidophila* strain 10050, *Rb. sphaeroides* 2.4.1, *Rhodopseudomonas palustris*, *Rhodospirillum* (*Rs.*) *rubrum* S1 and *Chromatium* (*C.*) *purpuratum* were grown photoheterotrophically under high light (150 μmol s^{-1} m^{-2}) conditions at a temperature of 28 ± 2°C. The thermotolerant species *Chromatium vinosum* strain D was grown under the same light conditions but at an elevated temperature of 40°C. Low light (LL) and low light/low temperature (LL/LT) *Rps. acidophila* strain 7750 was also grown at light intensities of about 40 μmol s^{-1} m^{-2} at 28°C or 22°C, respectively.

Chromatophores and photosynthetic membranes were prepared as described by Law et al. [34]. Preparation of *Rps. acidophila* strain 10050 LH2 complex is described in [35]. Chromatophores and membranes were suspended in 20 mM Tris, pH 8.0, and stored at −20°C until required. Optical cuvettes of 1 cm × 1 cm were used for all measurements.

2.2. Instrumentation

Quantum corrected fluorescence spectra were recorded at 24°C with a custom-built fluorimeter equipped with a Si-avalanche photodiode (APD) as the detector. The slit widths on the excitation and emission sides were 2 mm each. The cuvette holder was mounted 1 cm away from the excitation slit of the monochromator and the APD directly behind the emission slit. The monochromator contained a holographic grating with 1200 lines per mm. The Blaze wavelength was 750 nm. The excitation sources for the fluorescence spectra were provided by two pulsed laser diodes emitting narrow lines at 803 nm and 900 nm, respectively. Typically, the excitation lasted 500 μs and the fluorescence yield integrated over this time interval yielded one data point at any given wavelength. Usually nine such data points were averaged before the step motor advanced to the next wavelength. The repetition rate of excitation flashes was adjustable to any value. The fluorescence spectra obtained at each excitation wavelength were first scaled to each other at wavelength > 910 nm and then multiplied by a common factor chosen such that the maximum of the fluorescence matched the maximum of the absorption spectrum.

Absorption spectra were recorded on an Aminco DW2000 spectrophotometer in which the standard photomultiplier detector was replaced by a Si-APD. This allowed the recording of absorption spectra up to 1050 nm with good signal to noise ratio.

All experiments were performed at a room temperature (RT) of 23 ± 1°C.

3. Results

3.1. Control experiments

3.1.1. Absorption and fluorescence spectra from B800-850 and Rs. rubrum

As a first control experiment the absorption and fluorescence emission spectra of isolated LH2 (B800-850) from *Rps. acidophila* strain 10050, which was solubilized in 20 mM Tris-HCl, pH 8.0, containing 0.1% (v/v) lauryl dimethylamine-*N*-oxide (LDAO), were measured (Fig. 1a). The absorption spectrum displayed two peaks at around 800 nm and 860 nm. Within the signal to noise ratio the fluorescence spectrum was independent of the excitation wavelength (803 nm versus 900 nm). The scattering artifact upon 900 nm excitation (arrow) extends over three data points, corresponding to 6 nm.

As a second control experiment the absorption and fluorescence emission spectra of chromatophores from the LH1-RC only species *Rs. rubrum* were measured (Fig. 1b). The absorption spectrum displayed only one strong peak at around 880 nm. Within the signal to noise ratio this fluorescence spectrum was also independent of the excitation wavelength (803 nm versus 900 nm).

3.1.2. Spectral decomposition

None of the above absorption peaks had the shape of a single Gaussian function. Therefore, a spectral decomposition was performed by describing each of the absorption bands (B800, B850 and B880) on a wave number scale by a set of coupled Gaussian functions according to:

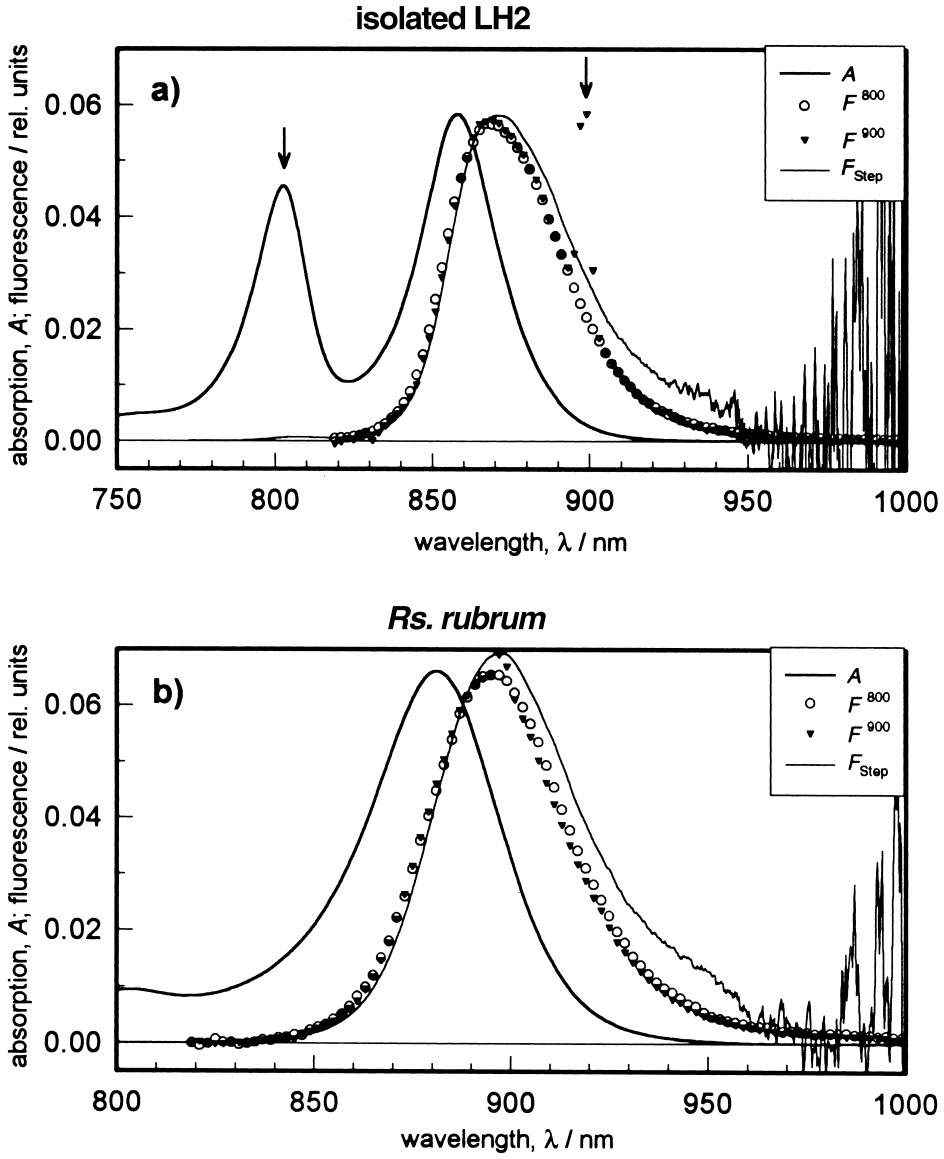

Fig. 1. (a) Absorption (thick solid line) and fluorescence spectra (○ and ▼) of the isolated LH2 complex at two excitation wavelengths as indicated. Transformation of the absorption spectrum according to the Stepanov relation (thin solid line). (b) Absorption (thick solid line) and fluorescence spectra (○ and ▼) of *Rs. rubrum* chromatophores at two excitation wavelengths as indicated. Transformation of the absorption spectrum according to the Stepanov relation (thin solid line).

$$A(\nu,\nu_{max},\beta) = \frac{1}{\sum_j a_j}\left(\sum_j \frac{a_j}{\sqrt{2\pi}\Delta\nu_j\beta} e^{-\left(\frac{\nu_{max}(1+\alpha_j\beta)-\nu}{\sqrt{2}\Delta\nu_j\beta}\right)^2}\right) \quad (1)$$

With this band function, A, one can describe the shape of an absorption band by the empirical fit parameters ν_{max}, a_j, α_j, and $\Delta\nu_j$, under the special condition $\beta = 1$. The function has a normalized area of one ($\int_{-\infty}^{\infty} A(\nu,\nu_{max},\beta)d\nu = 1$) independent of any particular choice of parameters like the position of the absorption maximum or the width of the band. The advantage of this function is its ease of use in fitting other related absorption bands by simply two parameters, namely a new maximum by ν_{max} and a new width by β. The particular combination of terms in Eq. 1 allows one both to shift and to narrow the band (with the parameters ν_{max} and β, respectively)

without changing the characteristic band shape. It is also worth mentioning that the normalization of A to 1 implies an invariant oscillator strength [36].

To describe the absorption spectrum of the LH1-RC only purple bacterium *Rs. rubrum* we used three spectral pools in order to account for the three pigment types involved, B880, the primary donor P875 and the 800 nm absorbing accessory BChls. The shape of the latter two bands was estimated by simple Gaussians with the parameters listed in Table 1. For a good fit of the B880 absorption band between 780 nm and 970 nm six coupled Gaussian functions in Eq. 1 ($j=6$) were needed (parameters in Table 1). This set of parameters defined the term A_{B880} used for the spectral decomposition of other complexes.

To test the applicability of the B880 band function it was used to fit the absorption spectrum of the B800-850 complex in the range 780–950 nm (Fig. 1a). This was done with two separate band functions for B800 and B850 to account for the different widths of the two peaks. The fit quality was high in the range 780–880 nm but noticeable deviations occurred at wavelengths longer than 880 nm where the real absorption was slightly larger than the best fit curve (data not shown). The best fit yielded a ratio of the oscillator strength of $f_{B850}/f_{B800}=2\pm0.05$. The aforementioned deviations show that the band shapes of B880 (used for the fit) and B850 are different at the red wings. Therefore, for further analysis we fitted the B850 and B800 bands by two further band functions (parameters in Table 1) using the restriction $f_{B850}/f_{B800}=2$. This yielded A_{B800} and A_{B850} used for the decomposition of the absorption spectra of the LH2-containing purple bacteria.

Table 1
Decomposition with Gaussian bands according to Eq. 1 of B800 and B850 from isolated LH2 from *Rps. acidophila* and of LH1 from *Rs. rubrum*

	a_j	α_j	$\Delta\nu_j/cm^{-1}$
LH2-B800	1	0	110
($\nu_{max}=12\,461$ cm^{-1})	0.20	−0.004	176
($\lambda_{max}=802.5$ nm)	0.26	0.019	110
	0.3	0.050	242
LH2-B850	1	0	147
($\nu_{max}=11\,658$ cm^{-1})	0.100	0.070	235.2
($\lambda_{max}=857.8$ nm)	0.085	0.028	117.6
	0.300	0.006	338.1
	0.092	−0.0248	102.9
	0.017	−0.042	102.9
	0.025	0.040	117.6
LH1-*Rs. rubrum*	1	0	177
($\nu_{max}=11\,342$ cm^{-1})	0.160	0.100	189.4
($\lambda_{max}=881.7$ nm)	0.125	0.0615	185.8
	0.255	0.0305	173.5
	0.070	−0.027	159.3
	0.013	−0.048	212.4
P875-RC	2	0	330
($\nu_{max}=11\,429$ cm^{-1})	2	0.093	165
($\lambda_{max}=875$ nm)			

Thus, the spectral decomposition of the absorption of the LH2+LH1 purple bacteria studied was performed with four normalized band functions, namely $A_{B800}(\lambda)$, $A_{B850}(\lambda)$, $A_{B880}(\lambda)$, and $A_{RC}(\lambda)$. Then the absorption spectrum of a PSU, which may also contain B820 and B830 complexes at the proper stoichiometric ratios, can be quantitatively described by:

$$A(\lambda) = N_{B800}\cdot A_{B800}(\lambda) + N_{B820}\cdot A_{B820}(\lambda) + N_{B830}\cdot A_{B830}(\lambda) + N_{B850}\cdot A_{B850}(\lambda) + N_{B880}\cdot A_{B880}(\lambda) + A_{RC}(\lambda) \quad (2)$$

For the practical application of Eq. 2, $A(\lambda)$ was normalized at a convenient wavelength to the experimental spectrum.

The quantitative fit of the absorption spectrum of an LH2-LH1-RC system was performed by assigning 32 absorbing pigments to the B880 band ($N_{B880}=32$) and four pigments to the RC ($N_{RC}=4$; two for primary donor at 875 nm and two for the accessory BChls at 800 nm) and assuming fixed ratios of $N_{B820}/N_{B800}=N_{B830}/N_{B800}=N_{B850}/N_{B800}=2$. The number of peripheral rings was then calculated under the assumption that one LH2 ring contains nine B800 molecules [7,37], i.e. $N_{ring}=N_{B800}/9$.

3.1.3. Stepanov relation

The Stepanov equation, which relates absorption and fluorescence spectra of thermally equilibrated chromophores or chromophore systems, has been frequently applied to photosynthetic systems [38–42]. The requirements for the validity of the Stepanov relation are super fast intra- and inter-molecular thermalization [43–45]. This seems to be met both in isolated LH2 because of the fast B800 → B850 energy transfer and long excited state lifetime of approx. 1 ns [46] and also in the LH1-RC system of *Rs. rubrum*

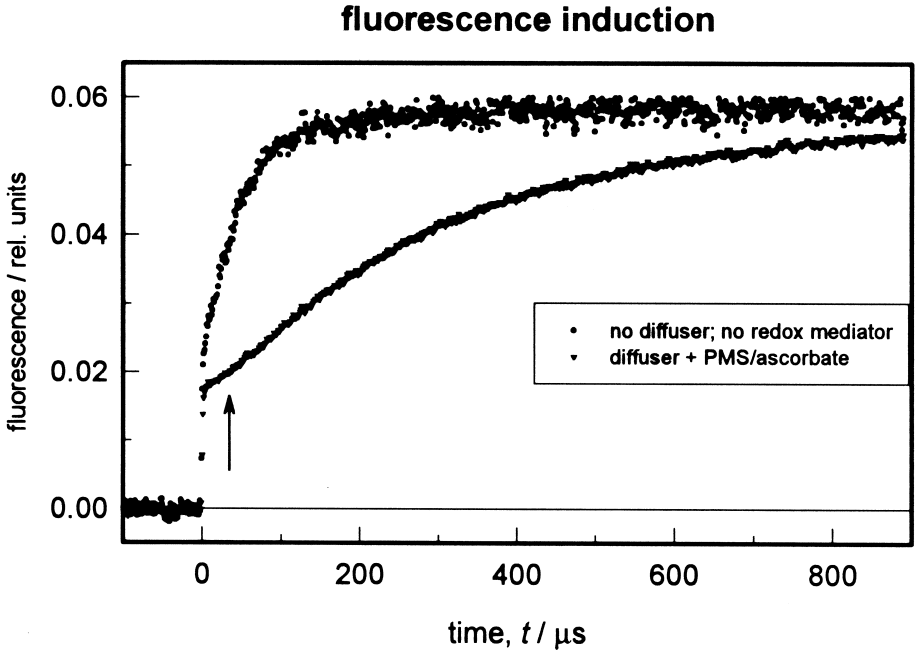

Fig. 2. Fluorescence induction curves of *Rs. rubrum* chromatophores upon excitation at 900 nm without diffuser and without redox mediators (noisy curve; single shot) and with diffuser and 2 μM PMS+10 mM ascorbate (less noisy curve; ten traces averaged). The arrow is positioned at 30 μs after the onset of the illumination and indicates the end of the light exposure for the F_o condition.

because of the very rapid (<1 ps) equilibration within the LH1 ring [6,47–50] which is much shorter than the excited state lifetime (≈ 70 ps) [51]. However, application of the Stepanov relation to these two examples showed significant deviations between the theoretical fluorescence spectra (calculated by the Stepanov relation) and the experimentally measured fluorescence spectra (Fig. 1). When normalized near the fluorescence maxima the theoretical spectra showed too little intensity at the hypsochromic side and too much intensity at the bathochromic side. Such deviations could indicate a pigment system in which not all pigments contribute with the same fluorescence yield. This situation actually occurs in the LH1-RC system because the 880 nm absorption band is composed of differently fluorescing chromophores, the B880 antenna pigments and the BChl *a* of the special pair in the RC. The fluorescence quantum yield of the B880 pigments is high (corresponding to 60–80 ps excited state lifetime) whereas that of the special pair is very low (corresponding to 3 ps excited state lifetime). In other words, all 34 BChl *a* contribute to the absorption band but only 32 pigments to the fluorescence. This pigment heterogeneity becomes 'visible' because the bandwidth of the special pair is broader than the bandwidth of B880, i.e. the two bands have different shapes and consequently different Stokes shifts. However, the Stepanov transformation of the absorption spectrum in which the RC absorption was subtracted also did not match the measured fluorescence spectrum (data not shown).

On the other hand, in the case of LH2 the above explanation is not conceivable for the poor quality of the Stepanov relation. Fluorescence re-absorption due to too concentrated solutions can be excluded as a possible source of error, since in this case the measured fluorescence intensity in the vicinity of the absorption maximum would be lower and not higher than that predicted by the Stepanov relation.

3.1.4. F_m and F_o conditions

As mentioned in Section 2 the excitation sources were laser diodes which were controlled by electronic circuitry to emit constant light of various durations. Typically the pulse length was 500 μs and the repetition rate was 1 Hz. The laser beam had a profile of approx. 2×4 mm (centered to the middle of the cuvette). If no redox chemicals were added to the chromatophores this excitation established conditions in

which the primary donor was in the oxidized state (F_m conditions). This was demonstrated for *Rs. rubrum* chromatophores by recording the time-resolved fluorescence change of a dark-adapted sample (Fig. 2). The single shot rise kinetics of the fluorescence from F_o to F_m occurs within 100 μs (Fig. 2, upper curve). At the repetition rate of 1 Hz the induction started with a value very close to F_m. Therefore, all fluorescence spectra recorded under these standard conditions represent F_m spectra.

To achieve F_o conditions in which essentially all RCs are open we added 10 mM ascorbate and 2 μM phenazine methosulfate (PMS) to the sample. In addition it was necessary to homogenize the laser beam

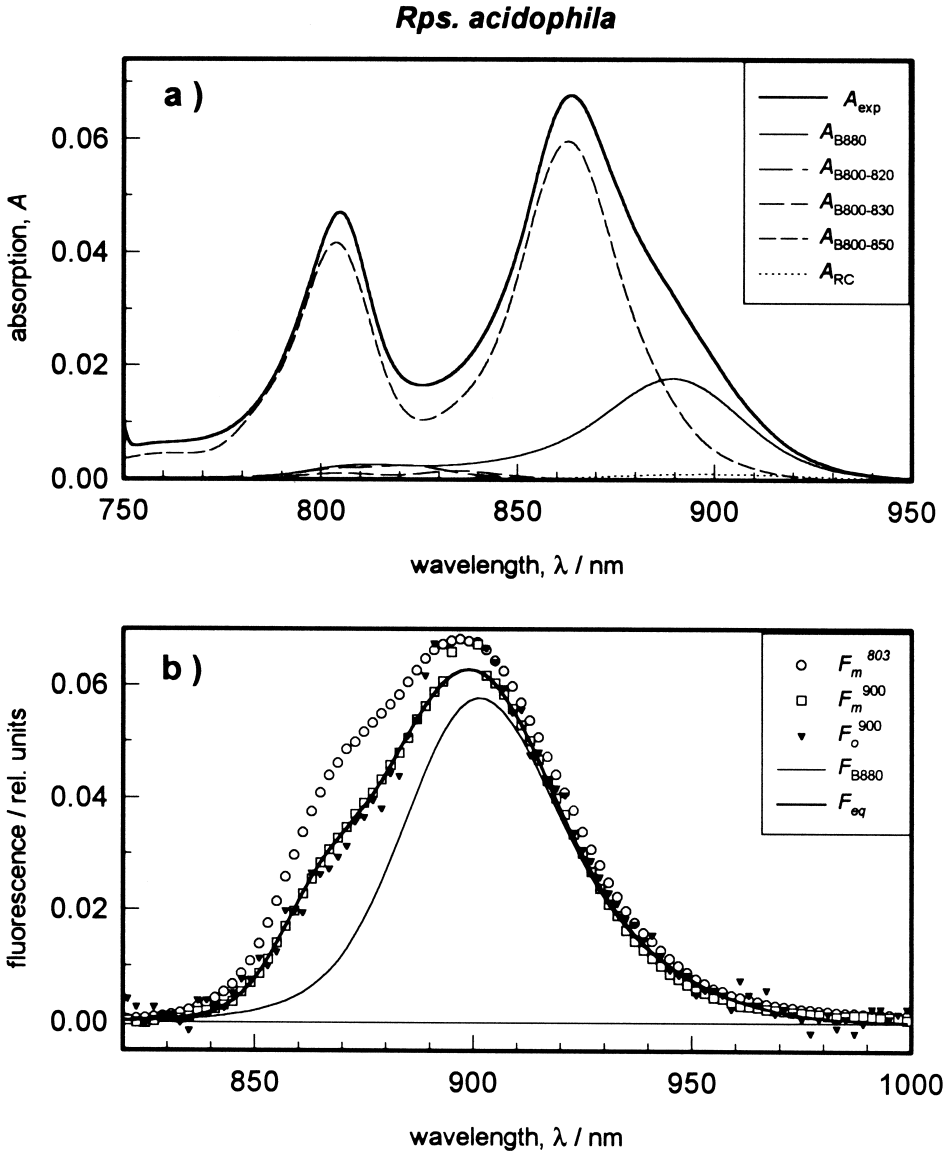

Fig. 3. *Rps. acidophila* chromatophores. (a) Absorption spectrum (thick solid line) and its spectral decomposition into B800-820, B800-830, B800-850, B880 and RC complexes as described in the text and listed in Table 2. (b) Fluorescence spectra upon excitation at 803 nm and 900 nm under F_o and F_m conditions (various symbols) as well as the theoretical fluorescence spectrum (thick solid line) constructed under the assumption of a Boltzmann distribution among the pigment pools quantified in Table 2. Also shown is the calculated emission from the B880 complex alone (thin solid line). The theoretical fluorescence spectrum was scaled to yield a maximal amplitude corresponding to the absorption of the sample and the experimental fluorescence spectra were then adjusted to the theoretical one by eye to give reasonable overlap.

by a diffuser plate. This resulted both in slower fluorescence induction kinetics and in superimposable traces up to 10 Hz (Fig. 2, lower trace). To record F_o fluorescence spectra the pulse duration was reduced to 30 μs. During this short time only a negligible fraction of RCs become closed as indicated by the arrow in Fig. 2.

3.2. Absorption and fluorescence spectra of LH2+LH1 purple bacteria

3.2.1. Rps. acidophila

The RT absorption and fluorescence spectra of a membrane preparation from *Rps. acidophila* grown under normal conditions are shown in Fig. 3. The spectral decomposition of the absorption spectrum (Fig. 3a) according to the procedure described above with respect to B800-B820, B800-B830, B800-850, B880 and RC yielded the stoichiometric ratios listed in Table 2 (fit parameters ν_{max} and β). The calculation is based on the assumption of equal oscillator strengths of the pigments and of 32 B880 ($N_{B880} = 32$), two primary donor BChls and two 800 nm absorbing accessory BChls ($N_{RC} = 4$) making up the core complex [36].

Although the number of B800-B820 and B800-B830 complexes is small these are needed to achieve a good fit. It should be emphasized that the introduction of B800-B830 complexes follows from the present concept of spectral decomposition (Eq. 1) and should not be taken as a proof for the physical existence of such a complex. It is just a way to account for the deviation of a particular band shape from our assumed standard band shape. This comment applies to all other minor peripheral complexes listed in Table 2, except *C. purpuratum*.

If all peripheral LH2 complexes (B800-B820, B800-B830, and B800-850) are assumed to be arranged in rings consisting of nine α,β-polypeptides each binding one B800 one can estimate the number of LH2 rings belonging to a PSU. In the case of *Rps. acidophila* grown under high light conditions there are 5.1 LH2 rings surrounding one LH1-RC (Table 2). In addition, Table 2 gives the absorption maxima of the pigment groups as they follow from the fit with Eq. 1.

The fluorescence spectra upon excitation at 803 nm and 900 nm under F_m conditions differed significantly at wavelengths < 910 nm (Fig. 3b; circles vs. squares) in that the fluorescence yield upon 803 nm was higher than that upon 900 nm excitation. When the 900 nm excitation was carried out under F_o conditions a very similar fluorescence spectrum to the F_m spectrum was obtained (Fig. 3b; triangles). The F_o spectrum scattered much more because of the strongly reduced light intensity and the lower fluorescence yield. Also, the scattering artifact at 900 nm was much more pronounced under F_o conditions because of the diffuser plate inserted in front of the cuvette. Nevertheless, it can be stated that the F_m and F_o fluorescence spectra upon 900 nm excitation agree within the signal to noise ratio (given by the F_o spectrum). Eventually, a slightly smaller amplitude of the F_o spectrum at around 875 nm could be traced. The interpretation of these results will be given in Section 4 where the fluorescence yields from the different pigment pools will be analyzed by equilibrium thermodynamics as well as by a kinetic scheme.

Table 2
Number of BChl molecules per PSU (= antenna size) according to the spectral decomposition described in the text as well as the position of the absorption maxima of the bands

Species	Antenna sizes of the PSU					Absorption maxima of the pigment pools/nm				
	N_{800}	N_{820}	N_{830}	N_{850}	$N_{LH2-rings}$	B800	B820	B830	B850	B880
Rps. acidophila	46	3	2	87	5.1	804	823	835	863	891
Rps. acidophila LL	54	36	9	62	5.9	802	823	837	862	891
Rps. acidophila LL/LT	54	66	17	25	6.0	800	826	841	861	892
Rps. palustris	20	2	1	36	2.2	806	820	838	861	882
Rb. sphaeroides 2.4.1	31	–	–	61	3.4	802	–	–	853	881
C. vinosum	20	2	–	37	2.2	806	820	–	863	883
C. purpuratum	71	–	141	–	7.8	802	–	832	–	877

The following stoichiometries were assumed: $N_{880} = 32$; $N_{RC} = 4$; $N_{LH2-rings} = N_{800}/9$.

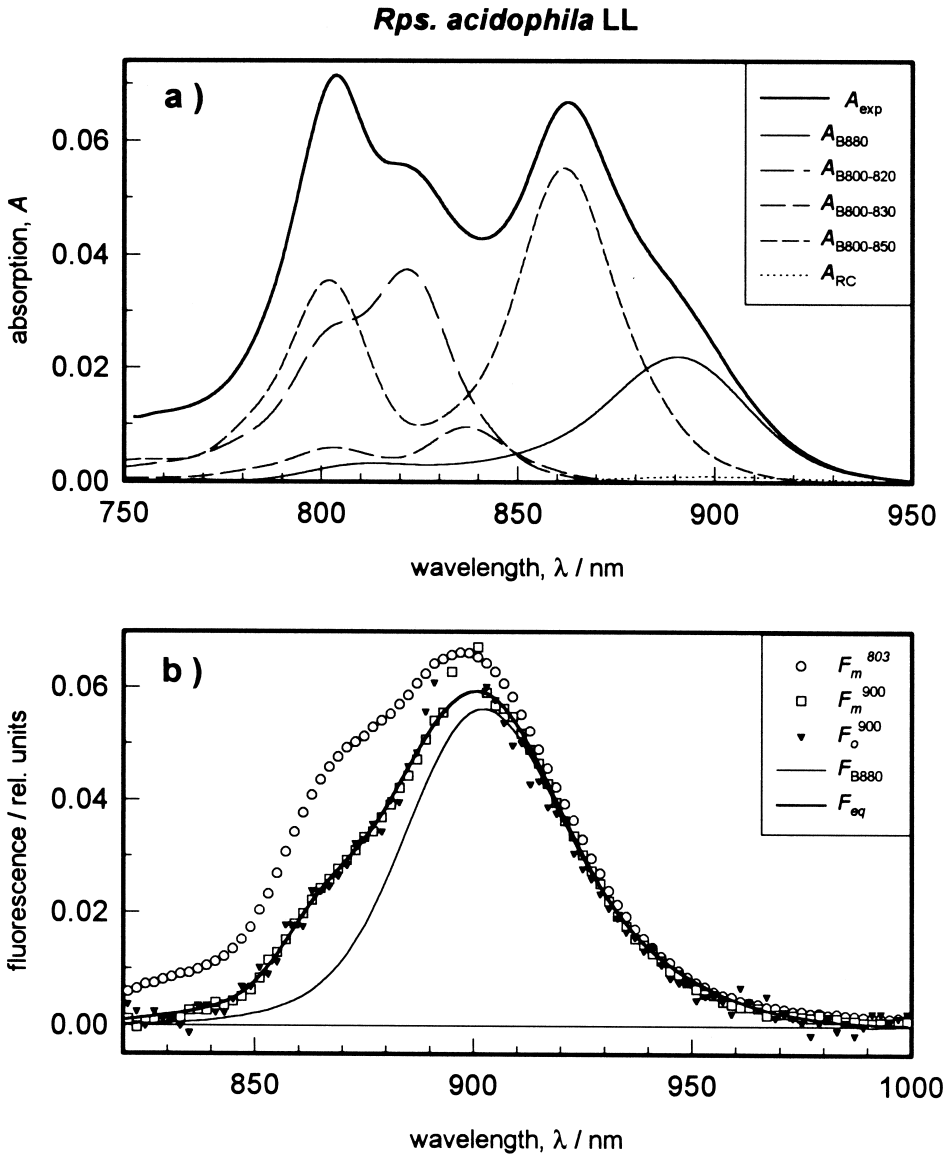

Fig. 4. *Rps. acidophila* LL chromatophores. (a) Absorption spectrum (thick solid line) and its spectral decomposition into B800-820, B800-830, B800-850, B880 and RC complexes as described in the text and listed in Table 2. (b) Fluorescence spectra upon excitation at 803 nm and 900 nm under F_o and F_m conditions (various symbols) as well as the theoretical fluorescence spectrum (thick solid line) constructed under the assumption of a Boltzmann distribution among the pigment pools quantified in Table 2. Also shown is the calculated emission from the B880 complex alone (thin solid line). The normalization of the fluorescence spectra is described in the legend of Fig. 3.

The analogous spectra of *Rps. acidophila* grown under LL and LL/LT conditions are shown in Figs. 4 and 5, respectively. In contrast to high light grown cells the LL cells possess a significant fraction of B800-B820 complexes in their antenna system as judged by the absorption peak at around 830 nm (Fig. 4a). In LL/LT cells the B800-B820 complexes are the dominant peripheral complexes (Fig. 5a). The number of LH2 rings in the LL cells is comparable with that of the LL/LT ones and both are higher than in the high light grown cells (Table 2). The typical features of the fluorescence spectra are the same as in high light grown cells (Fig. 3b and Fig. 5b).

3.2.2. *Rps. palustris*

The absorption spectrum of *Rps. palustris* shows

two peaks located near 805 nm and 860 nm with a weak shoulder located at about 880 nm (Fig. 6a). A good fit of the absorption spectrum required the assumption of the presence of a small number of B820 or B830 pigments. The total number of B800 pigments ($N_{B800} = 20$) is significantly smaller than the corresponding numbers found in *Rps. acidophila*. Given the assumptions described in the legend of Table 2, the number of B800 pigments equates to 2.2 LH2 rings per core complex.

Fig. 6b shows the fluorescence spectrum upon excitation at 803 nm (open circles) and 900 nm (open squares). These spectra were recorded under F_m conditions. The spectrum upon excitation at 900 nm and recorded under F_o conditions (filled triangles) was, within the scatter of the data points, the same as

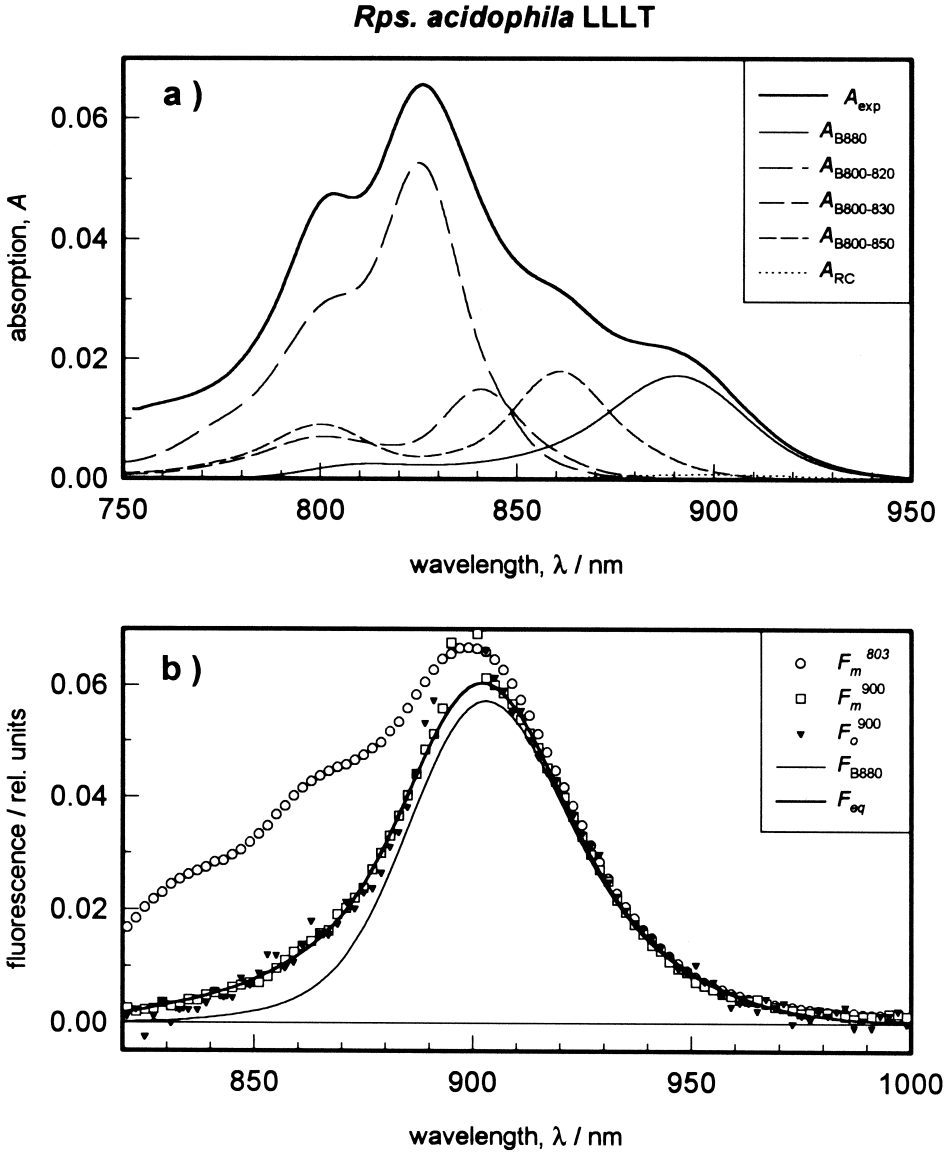

Fig. 5. *Rps. acidophila* LL/LT chromatophores. (a) Absorption spectrum (thick solid line) and its spectral decomposition into B800-820, B800-830, B800-850, B880 and RC complexes as described in the text and listed in Table 2. (b) Fluorescence spectra upon excitation at 803 nm and 900 nm under F_o and F_m conditions (various symbols) as well as the theoretical fluorescence spectrum (thick solid line) constructed under the assumption of a Boltzmann distribution among the pigment pools quantified in Table 2. Also shown is the calculated emission from the B880 complex alone (thin solid line). The normalization of the fluorescence spectra is described in the legend of Fig. 3.

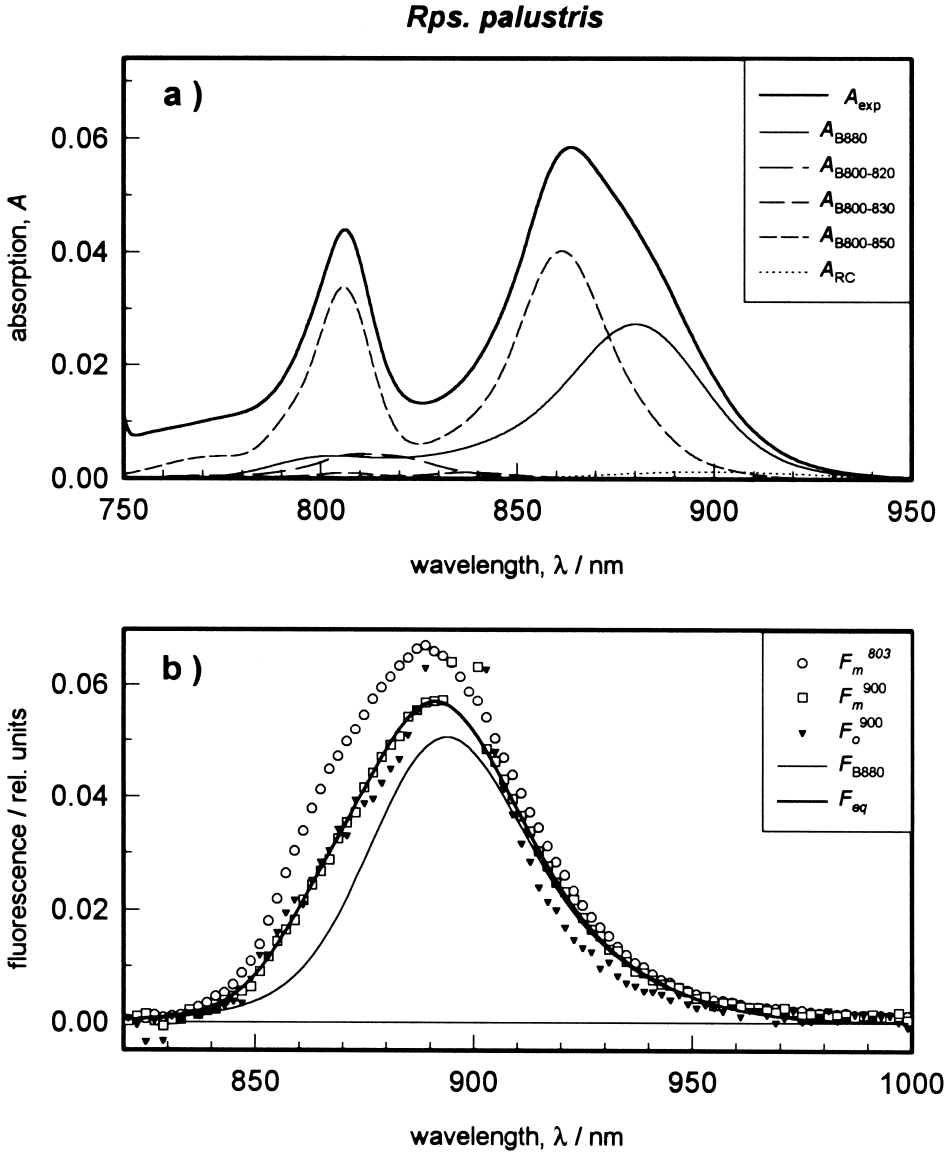

Fig. 6. *Rps. palustris* chromatophores. (a) Absorption spectrum (thick solid line) and its spectral decomposition into B800-820, B800-830, B800-850, B880 and RC complexes as described in the text and listed in Table 2. (b) Fluorescence spectra upon excitation at 803 nm and 900 nm under F_o and F_m conditions (various symbols) as well as the theoretical fluorescence spectrum (thick solid line) constructed under the assumption of a Boltzmann distribution among the pigment pools quantified in Table 2. Also shown is the calculated emission from the B880 complex alone (thin solid line). The normalization of the fluorescence spectra is described in the legend of Fig. 3.

the corresponding spectrum recorded under F_m conditions at wavelengths <880 nm but deviated slightly at wavelengths above this. The theoretical spectrum, based on the assumption of thermal equilibration (thick solid line), also matches these spectra at wavelengths <880 nm. The spectrum obtained under F_m conditions upon excitation at 803 nm (open circles) had a larger amplitude than both the theoretical spectrum and those obtained by 900 nm excitation at wavelengths <910 nm. However, it matched the theoretical spectrum and the spectrum recorded under F_m conditions upon excitation at 900 nm at wavelengths >910 nm.

3.2.3. *Rb. sphaeroides*

The absorption spectrum of *Rb. sphaeroides* strain

2.4.1 features two peaks located near 800 nm and 853 nm (Fig. 7a). There is a distinct shoulder located at about 880 nm. In this species the spectral decomposition could be performed without invoking the presence of B800-820 or B800-830 complexes. Compared to *Rps. acidophila* the absorption maximum of the core complex lies about 10 nm to the blue. As was the case with *Rps. palustris*, the total number of B800 pigments ($N_{B800} = 31$) is significantly smaller than the corresponding numbers found in *Rps. acidophila* and equates to 3.4 LH2 rings per core complex.

Fig. 7b shows the fluorescence spectrum upon excitation at 803 nm (open circles) and 900 nm (open squares). These spectra were recorded under F_m conditions and both show the presence of a shoulder at about 860 nm. The spectrum upon excitation at 900

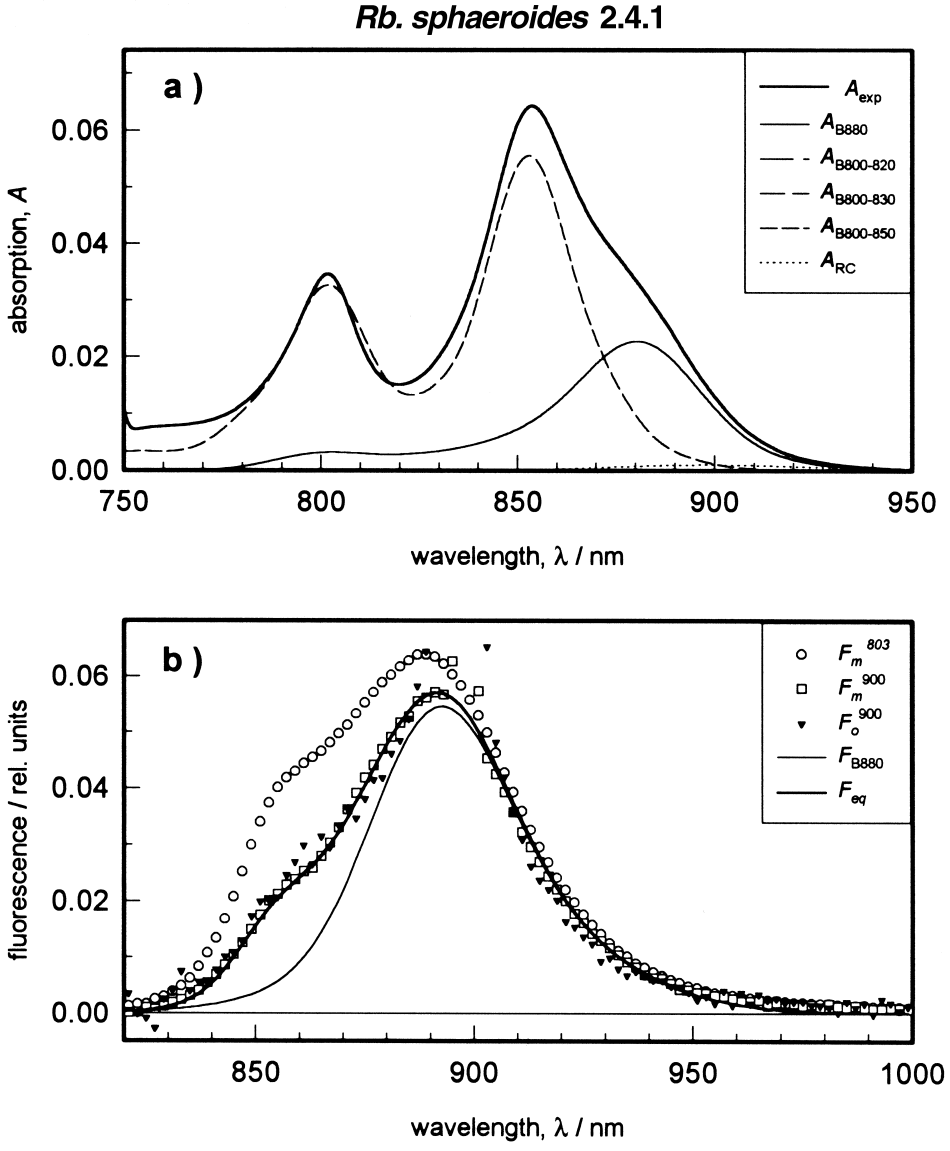

Fig. 7. *Rb. sphaeroides* 2.4.1 chromatophores. (a) Absorption spectrum (thick solid line) and its spectral decomposition into B800-820, B800-830, B800-850, B880 and RC complexes as described in the text and listed in Table 2. (b) Fluorescence spectra upon excitation at 803 nm and 900 nm under F_o and F_m conditions (various symbols) as well as the theoretical fluorescence spectrum (thick solid line) constructed under the assumption of a Boltzmann distribution among the pigment pools quantified in Table 2. Also shown is the calculated emission from the B880 complex alone (thin solid line). The normalization of the fluorescence spectra is described in the legend of Fig. 3.

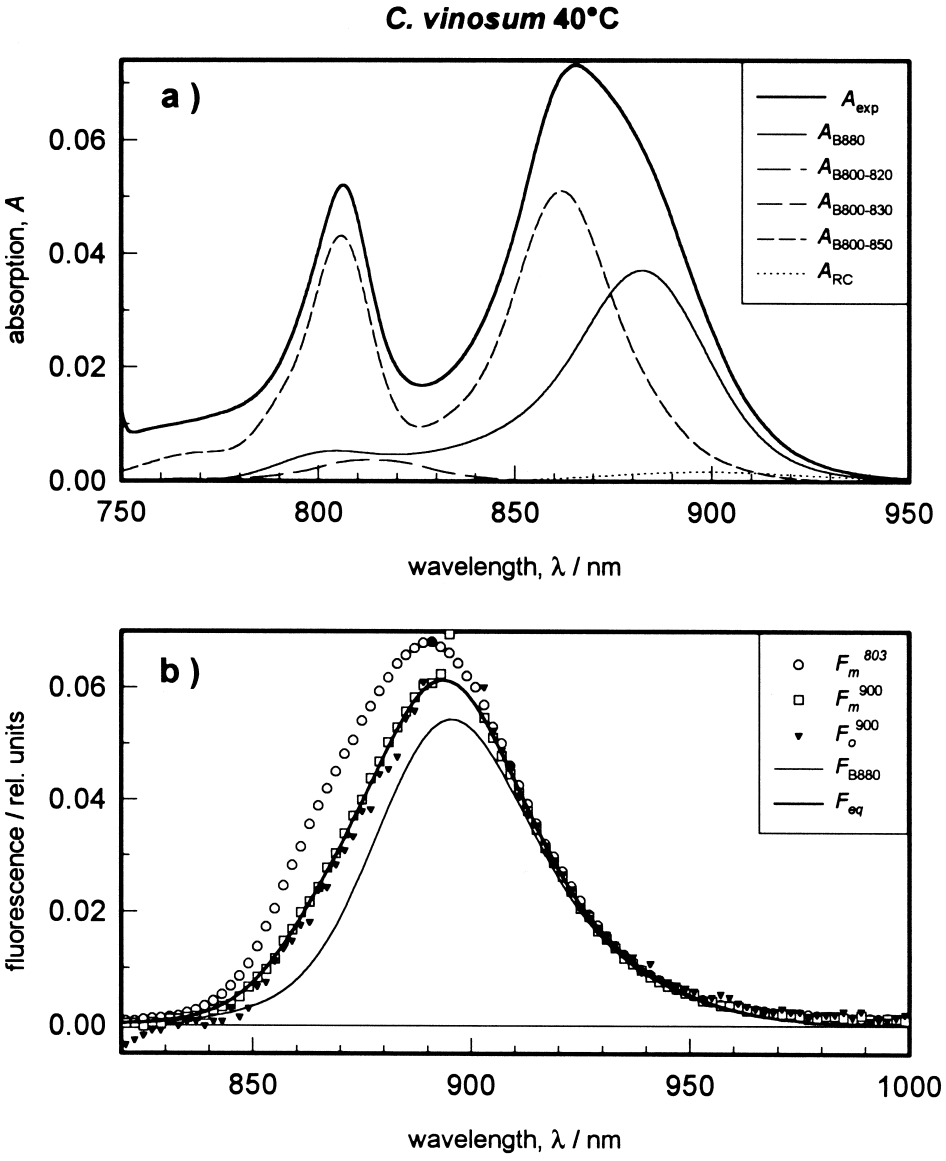

Fig. 8. *C. vinosum* chromatophores. (a) Absorption spectrum (thick solid line) and its spectral decomposition into B800-820, B800-830, B800-850, B880 and RC complexes as described in the text and listed in Table 2. (b) Fluorescence spectra upon excitation at 803 nm and 900 nm under F_o and F_m conditions (various symbols) as well as the theoretical fluorescence spectrum (thick solid line) constructed under the assumption of a Boltzmann distribution among the pigment pools quantified in Table 2. Also shown is the calculated emission from the B880 complex alone (thin solid line). The normalization of the fluorescence spectra is described in the legend of Fig. 3.

nm and recorded under F_o conditions was, within the scatter of the data points, the same as the corresponding spectrum recorded under F_m conditions. The theoretical spectrum also matches these spectra. However, the latter three spectra differ significantly from the spectrum obtained upon excitation at 803 nm.

3.2.4. *C. vinosum strain D*

The absorption spectrum of *C. vinosum* strain D shows two absorption peaks located near 805 nm and 865 nm with a broad shoulder located to the red of the latter peak (Fig. 8a). The spectral decomposition could be performed without invoking the presence of 830 nm absorbing pigments but did re-

quire the presence of 820 nm absorbing pigments. The total number of B800 pigments ($N_{B800} = 20$) was the same as that found in *Rps. palustris*. Again, this number of B800 pigments equates to 2.2 LH2 rings per core complex.

Both the fluorescence spectra obtained upon excitation at 900 nm and the theoretical spectrum show good agreement (Fig. 8b). However, the fluorescence spectrum upon excitation at 803 nm (open circles) has a larger amplitude than the other spectra between about 850 nm and 910 nm. At wavelengths >910 nm there is a good match of all spectra.

3.2.5. *C. purpuratum*

C. purpuratum is an unusual species of purple bac-

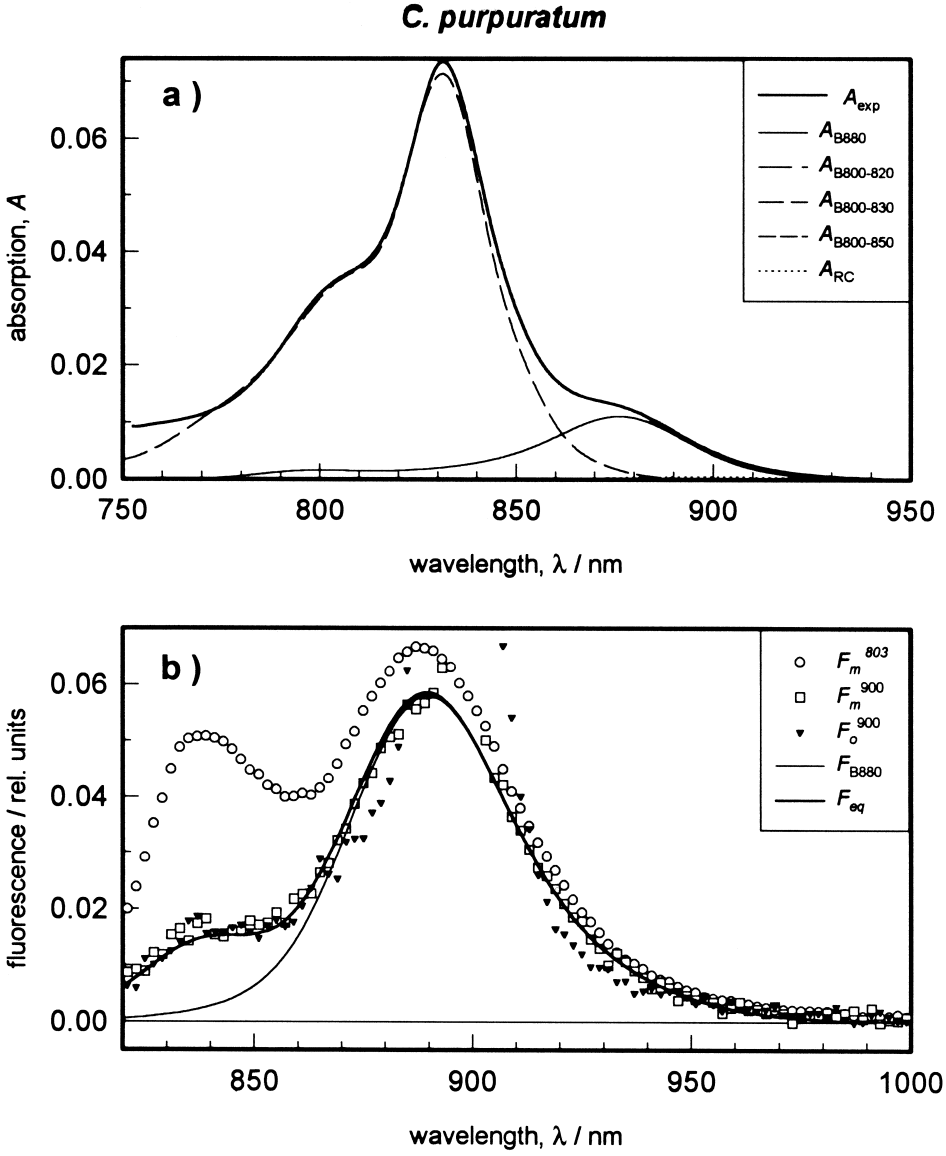

Fig. 9. *C. purpuratum* chromatophores. (a) Absorption spectrum (thick solid line) and its spectral decomposition into B800-820, B800-830, B800-850, B880 and RC complexes as described in the text and listed in Table 2. (b) Fluorescence spectra upon excitation at 803 nm and 900 nm under F_o and F_m conditions (various symbols) as well as the theoretical fluorescence spectrum (thick solid line) constructed under the assumption of a Boltzmann distribution among the pigment pools quantified in Table 2. Also shown is the calculated emission from the B880 complex alone (thin solid line). The normalization of the fluorescence spectra is described in the legend of Fig. 3.

teria in that it synthesizes a B800-830 complex as the only peripheral light-harvesting complex [52].

In contrast to the other species investigated the absorption spectrum of *C. purpuratum* features only a single NIR absorption peak located near 830 nm (Fig. 9a). There are distinct, broad shoulders located at about 800 nm and 880 nm. In this species the spectral decomposition was fitted only with B800-830 complexes. It was not possible to achieve a good fit if the presence of B800-850 or B800-820 complexes was assumed. This demonstrates the effectiveness of the methodology of the spectral decomposition. The total number of B800 pigments ($N_{B800} = 71$) is significantly larger than the corresponding numbers found in all the other species studied. This equates to 7.8 LH2 rings per core complex which is very close to the idealized number of eight.

The fluorescence spectra recorded under F_m conditions upon excitation at 803 nm (open circles) and 900 nm (open squares) are shown in Fig. 9b. These spectra deviate significantly at wavelengths < 910 nm. The most dramatic deviation is observed between about 830 nm and 890 nm. The spectrum recorded under F_o conditions upon excitation at 900 nm (filled triangles) was, within the scatter of the data points, similar to the corresponding spectrum recorded under F_m conditions but with slight deviations between about 870–890 nm and 920–940 nm. The theoretical spectrum (thick solid line) was the same as the spectrum recorded under F_m conditions upon excitation at 900 nm but deviated to a lesser or greater extent from the spectrum recorded under F_o conditions upon excitation at 900 nm and the spectrum recorded upon excitation at 803 nm, respectively. In our opinion the scatter of the data points does not allow one to determine whether the observed deviations are systematic or not.

4. Discussion

4.1. Antenna sizes

The antenna structure of the PSU in LL-*Rps. acidophila* was suggested to consist of eight LH2 rings that surround an LH1-RC complex [5]. According to our spectral decomposition of the absorption bands, which assumed an invariable oscillator strength of all pigments and 32 BChl in an LH1 ring, the number of LH2 rings in *Rps. acidophila* is smaller than the maximal, idealized ring number of eight, irrespective of the conditions under which this bacterium was grown (Table 2). Smaller ring numbers were also calculated for *Rps. palustris*, *Rb. sphaeroides*, and *C. vinosum*. Only in the case of *C. purpuratum* was the idealized number of eight found. However, if the number of BChl in an LH1 ring were smaller, as suggested by the work of Francke and Amesz [53], the antenna sizes of the peripheral complexes (Table 2) were inversely larger. Assumed that LH1 contains only 24 BChls due to the replacement of three α,β-heterodimers by *pufX* [54–56] the ring numbers would be underestimated by maximally 33%. This would lift the ring numbers in *Rps. acidophila* close to eight. However, the ring numbers in *Rps. palustris*, *Rb. sphaeroides* and *C. vinosum* would still be significantly smaller than eight. In any case in reality the perfect geometric arrangement of the core and peripheral ring complexes depicted by Papiz et al. [5] seems to be given only in special cases.

4.2. Possible contribution of free BChl

It might be suspected that the fluorescence spectra between 820 nm and 860 nm might be affected by free BChl present in the membranes of purple bacteria. Such a contamination can be excluded for several reasons. First, the absorption maximum of free BChl *a* lies at 770 nm. This means that at our excitation wavelength of 803 nm (and particularly at 900 nm) the excitation of free BChl is negligible. Second, the interference of our fluorescence spectra from *Rps. acidophila*, *Rps. palustris*, *Rb. sphaeroides* and *C. vinosum* by free BChl is negligible since no emission at 820 nm was measured (Fig. 3b, 6b, 7b and 8b). In the other cases the contribution of free BChl must be also small since free BChl *a* emits maximally at around 780 nm with a bathochromic emission that decreases with increasing wavelengths. However, our *F* spectra increase with wavelengths > 820 nm. Third, even if the 820 nm emission would be subtracted this would not cure the difference at 860 nm used for the following argumentation.

4.3. Theoretical simulations

4.3.1. Thermal equilibrium

From the decomposition of the antenna system into B800, B820, B830, B850, B880, and RC it is clear that the 900 nm light selectively excites LH1 and that the hypsochromic fluorescence shoulders (around 850–870 nm) originate from LH2, i.e. from exciton transfer LH1 → LH2. This demonstrates the existence of uphill energy transfer but not its quantification. In the following we investigate the hypothetical case of perfect thermalization.

4.3.1.1. Stepanov relation. For thermally equilibrated systems the Stepanov relation predicts the fluorescence spectrum from the absorption spectrum and vice versa [43–45]. Its validity depends critically on super fast intra- and inter-molecular thermalization, which seems to be given in both isolated LH2 because of the fast B800 → B850 energy transfer and long excited state lifetime of approx. 1 ns [46], and also in the LH1-RC system like that of *Rs. rubrum* because of the very rapid (<1 ps) equilibration within the LH1 ring [49,50] being much shorter than the excited state lifetime (≈ 70 ps) [51]. However, application of the Stepanov relation to these two examples showed systematic deviations between the theoretical fluorescence spectra calculated by the Stepanov relation and the measured fluorescence spectra (Fig. 1 and [38]) which makes the relation unsuited for the further analysis of LH2-containing purple bacteria. A similar discrepancy has also been noted by Zankel and Clayton [4].

The failure of the Stepanov relation in the case of the ring shaped light-harvesting complexes of purple bacteria is most likely due to the energetic imperfection of the rings (energetic disorder). Quantum mechanical calculations for a perfect (no energetic disorder) circular aggregate have shown that the transition from the ground state to the lowest excitonic state is forbidden and that the next two higher states carry all the oscillator strength [36,57–59]. However, in reality these rings are not perfect. Energetic disorder destroys the delocalized states which become more and more localized [60]. Also, the redmost states in the spectrum are the most localized [47,58]. Finally, the more localized the states are, the lower the oscillator strength will be. As the radiative rate decreases with decreasing oscillator strength, the fluorescence yield is not constant over the emission band but displays lower yields at longer wavelengths. In accordance with this explanation, for all purple bacteria investigated the absorption spectrum obtained by the Stepanov transformation of the measured fluorescence spectrum displayed lower values (10–20%) in the range 875–930 nm than the measured absorption spectra (data not shown).

Because the Stepanov relation turned out to be inappropriate for our analysis, we decided to analyze our fluorescence spectra by assigning each pigment pool its own fluorescence spectrum and to calculate the emission probabilities either by a Boltzmann term (thermal equilibration) or by a kinetic scheme (Section 4.3.2).

4.3.1.2. Boltzmann calculation. Using the spectral decomposition described in Section 3.1.2 one knows the number of pigments in each spectral pool of the PSU (Table 2) and, therefore, one can calculate the thermal equilibrium distribution of an exciton. If i denotes the spectral pool, N_i the number of pigments in the ith pool, and E_i the energy corresponding to the absorption maximum of the ith pool the probability for an exciton to reside in a particular spectral pool is given by the distribution function:

$$p_i = \frac{N_i \cdot e^{-\frac{E_i - E_1}{k_B T}}}{\sum_i N_i \cdot e^{-\frac{E_i - E_1}{k_B T}}} \tag{3}$$

Then, if $F_i(\lambda)$ denotes the fluorescence spectrum of a spectral pool normalized to the area of 1 the theoretically predicted equilibrium fluorescence spectrum can be calculated according to:

$$F(\lambda) = \sum_i p_i \cdot F_i(\lambda) \tag{4}$$

To proceed we fitted each of the fluorescence spectra of isolated LH2 and of *Rs. rubrum* with three Gaussian-coupled bands defined by Eq. 1 and used these two spectra as standards for the emission from LH2 (i.e. B820, B830, and B850) and LH1 (i.e. B880) of the LH2+LH1 purple bacteria studied. The maximum wavelengths were Stokes shifted by 50–80

cm^{-1} compared to the absorption maxima (Table 2) and the emission bandwidths slightly adjusted ($\pm 10\%$) to obtain good fits. Such calculated fluorescence spectra – using the parameters given in Table 2 – are shown as thick solid lines in Fig. 3b, 4b, 5b, 6b, 7b, 8b, 9b. In all the purple bacteria studied these equilibrium fluorescence spectra – ultimately derived from the spectral decomposition – agreed with the experimental fluorescence spectra upon 900 nm excitation (Fig. 3b, 4b, 5b, 6b, 7b, 8b, 9b). Thus, it can be concluded that the main part of the antenna system is thermally equilibrated and that uphill energy transfer occurs up to its thermodynamically maximal possible extent.

The above treatment also allows calculation of the predicted fluorescence spectra of each of the pigment pools, in particular those of the core complexes alone. These latter spectra are shown as thin solid lines in Fig. 3b, 4b, 5b, 6b, 7b, 8b, 9b. Comparison of these spectra with the measured fluorescence spectra allows one to judge the presence of uphill energy transfer. In all the purple bacteria studied the deviations between both spectra indicated significant uphill energy transfer (Fig. 3b, 4b, 5b, 6b, 7b, 8b, 9b).

4.3.2. Kinetic consideration

If a system were perfectly equilibrated both 803 nm and 900 nm excitations are expected to yield the same fluorescence spectrum. However, 803 nm excitation leads to excess emission from LH2 as evident from the larger fluorescence yield between 840 nm and 910 nm. This excess emission must stem either from the retardation caused by the B850 → B880 transfer or from poorly coupled or possibly even isolated LH2 rings. In order to distinguish between both possibilities a detailed kinetic analysis was performed.

In LH1+LH2-containing purple bacteria fluorescence is emitted predominantly by B850 and B880. Compared to the fluorescence yields of B850 or B880 the emission from B800 is negligible small due to the short excited state lifetime of <1 ps [18,20]. The same holds for the emission from the RC because in open RCs P* decays within approx. 3 ps [61] and in closed RCs P^+ is known to be non-fluorescent. Neglecting the emission from B800 and the RC, the relevant reaction scheme is:

$$D \xleftarrow{k_\ell} \mathrm{B850} \underset{k_{-1}}{\overset{k_1}{\rightleftarrows}} \mathrm{B880} \xrightarrow{k_{o,c}} C$$

in which the rate constant k_ℓ stands for losses of the B850 antenna into the ground state and the rate constants $k_{o,c}$ for losses of the B880 antenna by the open (P) or closed (P^+) RC, respectively. As derived in the Appendix the fluorescence yields of B850 and B880 complexes upon excitation in B850 are:

$$F^{\mathrm{B850}} = \frac{a_1}{\gamma_1} + \frac{a_2}{\gamma_2} \tag{5a}$$

$$F^{\mathrm{B880}} = \frac{k_1}{\gamma_1 \cdot \gamma_2} \tag{5b}$$

using the identification $k_2 = k_{o,c}$. The relation of the amplitude factors a_1 and a_2 as well as the apparent rate constants γ_1 and γ_2 to the molecular rate constants are also given in the Appendix. Then the ratio of fluorescence intensities is:

$$\left(\frac{F^{\mathrm{B880}}}{F^{\mathrm{B850}}}\right)_{850} = \frac{k_1}{a_1 \cdot \gamma_1 + a_2 \cdot \gamma_2} \tag{5c}$$

Upon excitation in the B880 complexes one obtains the fluorescence yields as derived in the Appendix:

$$F^{\mathrm{B850}} = \frac{k_{-1}}{\gamma_1 \cdot \gamma_2} \tag{6a}$$

$$F^{\mathrm{B880}} = \frac{a_1}{\gamma_2} + \frac{a_2}{\gamma_1} \tag{6b}$$

and for the ratio:

$$\left(\frac{F^{\mathrm{B880}}}{F^{\mathrm{B850}}}\right)_{880} = \frac{a_1 \cdot \gamma_1 + a_2 \cdot \gamma_2}{k_{-1}} \tag{6c}$$

Finally, the backward rate constant is related to the forward rate constant by the Boltzmann term according to

$$k_{-1} = k_1 \cdot \frac{N_{\mathrm{B850}}}{N_{\mathrm{B880}}} \cdot e^{\dfrac{E880 - E850}{k_B T}} \tag{7}$$

This latter equation accounts for the limiting case in which the correct thermal equilibrium is established in the absence of loss processes.

To investigate the influence of (i) the different excitation wavelengths, (ii) the different redox states of the RC and (iii) the departure from thermal equilibrium one has to assume reasonable numerical val-

ues for the rate constants. There is general agreement that $k_\ell = (1.0\ \text{ns})^{-1}$ [46] and that $k_{o,c} = (70\ \text{ps})^{-1}$, $(220\ \text{ps})^{-1}$ [51]. The rate constant for energy transfer from B850 to B880 is less certain, but in the range $k_1 = (3\text{–}30\ \text{ps})^{-1}$ [7,24]. For the following model calculations the upper and lower values for the B850 → B800 energy transfer ($k_1 = (3\ \text{ps})^{-1}$ and $k_1 = (30\ \text{ps})^{-1}$) were used in alternative calculations.

Given the above numbers and assuming $K = k_1/k_{-1} = 6$ one can plot the kinetics of the exciton distribution between B880 and B850 *upon excitation of B850* and fast energy transfer $k_1 = (3\ \text{ps})^{-1}$ for F_o conditions (Fig. 10a). It can be seen that the transfer equilibrium $\tilde{K}^0$ is reached within approx. 10 ps and that $\tilde{K}^0 = 5.80$ is only little smaller than the thermodynamic equilibrium constant $K = 6.00$. The situation is much different if the B850 → B800 energy transfer is assumed to be slower, $k_1 = (30\ \text{ps})^{-1}$. In this case the transfer equilibrium constant drops to $\tilde{K}^0 = 4.08$ as shown in Fig. 10b (in which the dependence of the various equilibrium values is plotted versus the speed of B850 → B800 energy transfer). More important, however, is the measurable quantity of the total fluorescence emitted by the two pigment pools, $(F^{B880}/F^{B850})_{850}$. These ratios are $(F^{B880}/F^{B850})_{850} = 4.77$ and $(F^{B880}/F^{B850})_{850} = 1.68$ for the fast and slow B850 → B800 energy transfer, respectively (Fig. 10b).

Next we investigated the case of *B880 excitation*. As shown in the Appendix the transfer equilibrium constant $\tilde{K}^0$ is independent of the excitation conditions. However, the measurable quantity of the ratio of the fluorescence yields of the two pigment pools, $(F^{B880}/F^{B850})_{880}$, now lies very close to (nearly indistinguishable from) the thermal equilibrium (Fig. 10b).

Having calculated the fluorescence yields from the different pigment pools it is straightforward to construct corresponding simulated fluorescence spectra. This is done in Fig. 10c for F_o conditions and in Fig. 10d for F_m conditions. For simplicity the emission bands of the B850 and B800 complexes are assumed to be Gaussians (Eq. 1; $j = 1$) with $\lambda_{max} = 850$ and $\lambda_{max} = 895$ and widths of $\sigma = 15$ nm. The total fluorescence spectra were normalized at their maximum. Fig. 10c and d compare the total fluorescence spectra upon B850 (upper solid curves) and B880 excitation (lower solid curves) as well as the two sub-bands (dashed and dotted curves) assuming *fast B850 → B800 energy transfer*. From these figures it can be seen that alternate excitation of the two complexes results in only small differences around 850 nm in the normalized fluorescence spectra. These differences are more pronounced under F_o than under F_m conditions (compare Fig. 10c and d) if, as mentioned previously, the B850 → B800 energy transfer is fast.

In a further model calculation, designed to simulate the experimental results, we compared the simulated F_o and F_m spectra – again normalized at their maximum – for excitation in B850 and B880 (Fig. 10e,f). If the *B850 → B800 energy transfer* is assumed to be *fast* (Fig. 10e) the deviations between the F_o spectra upon B850 and B880 excitation (solid line and points) are small as are the deviations between the F_m spectra upon B850 and B880 excitation (solid line and points). It is noteworthy that also the deviation between the F_o and the F_m spectrum is small.

However, if the *B850 → B800 energy transfer* is assumed to be *slow* (Fig. 10f) the deviations between the F_o spectra upon B850 and B880 excitation (solid line and points) are significant and the same applies for the deviations between the F_m spectra upon B850

→

Fig. 10. All calculations for this figure assumed a thermodynamic equilibrium constant of $K = 6$, which means that $k_{-1} = k_1/K$. All spectra are normalized at 985 nm. (a) Time dependence of the ratio of the instantaneous fluorescence yields $\tilde{K}(t)$ upon excitation in A, assuming open RCs with $k_2 = (70\ \text{ps})^{-1}$. (b) Dependence of the transfer equilibrium constant $\tilde{K}^0$ (thick dashed line) and the ratio of yields Φ_B/Φ_A (solid line) on the rate constant k_1 upon excitation in A, assuming open RCs with $k_2 = (70\ \text{ps})^{-1}$. Particular values for $k_1 = (3\ \text{ps})^{-1}$ and $k_1 = (30\ \text{ps})^{-1}$ are indicated with □. The ratio of yields Φ_B/Φ_A as a function of k_1 for excitation in B is the upper solid line and the particular values for $k_1 = (3\ \text{ps})^{-1}$ and $k_1 = (30\ \text{ps})^{-1}$ are indicated by ○. The thermodynamic equilibrium constant is indicated by the thin dashed line. (c) Simulated fluorescence spectra for $k_1 = (3\ \text{ps})^{-1}$ upon excitation in A (upper solid line) or B (lower solid line) under F_o conditions, i.e. $k_2 = (70\ \text{ps})^{-1}$. The dashed curves show the sub-bands imitating emission of A at 850 nm and B at 995 nm upon excitation in A and the dotted one the sub-band of A upon excitation in B. The sub-band of B upon excitation in B coincides with the dashed line upon excitation in A. (d) Same as in (c) except F_m conditions, i.e. $k_2 = (210\ \text{ps})^{-1}$. (e) Simulated fluorescence spectra for the case of fast energy transfer ($k_1 = (3\ \text{ps})^{-1}$) and excitation in A (solid lines) and B (dots) for F_o and F_m conditions, $k_2 = (70\ \text{ps})^{-1}$ and $k_2 = (210\ \text{ps})^{-1}$, respectively. (f) Same as in (e) but for the case of slow energy transfer ($k_1 = (30\ \text{ps})^{-1}$).

and B880 excitation (solid line and points). It is also notable that the deviation between the F_o and the F_m spectra is rather pronounced.

4.3.3. Comparison of simulations and experimental data

The above simulations, which are based on the

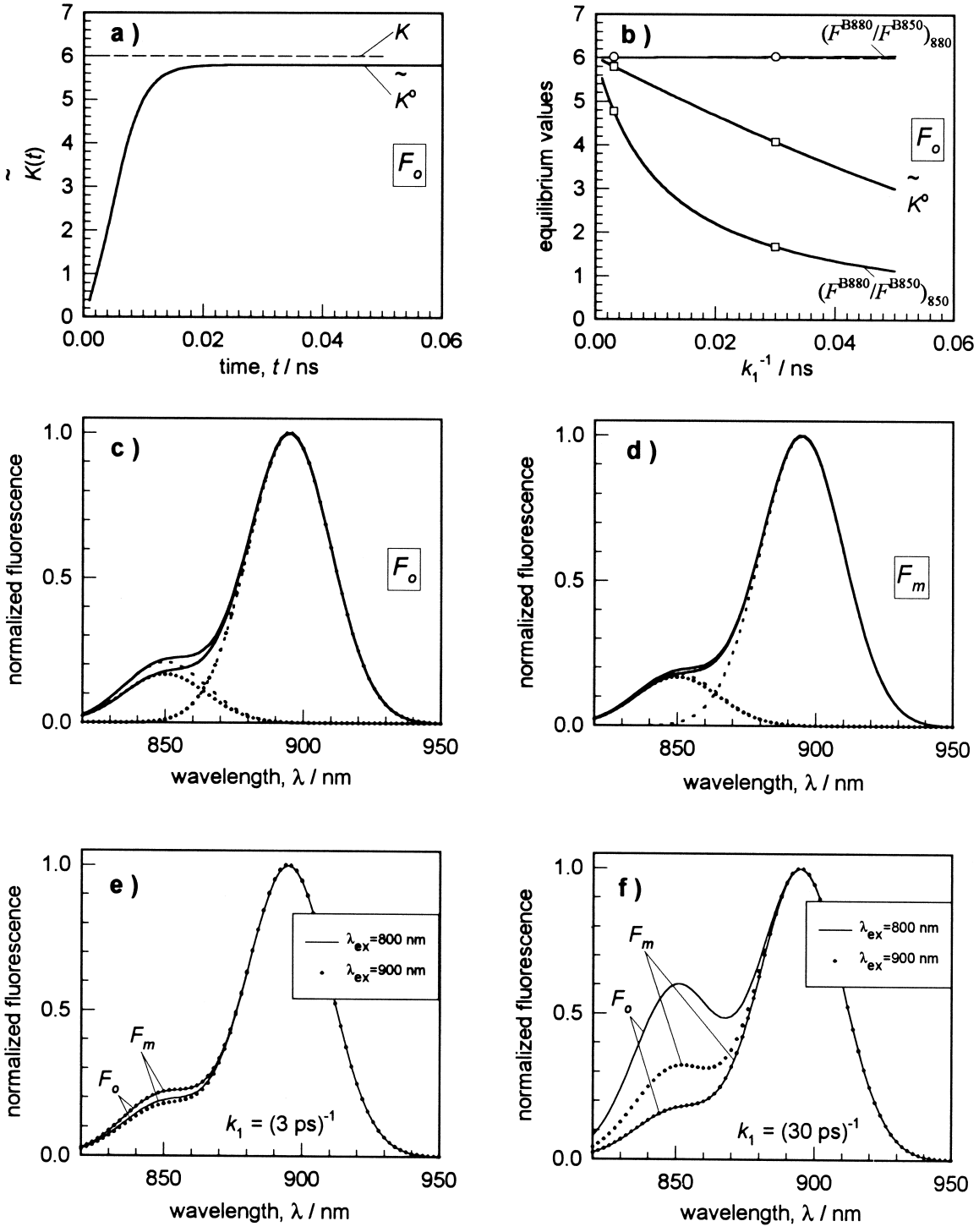

assumption of a homogeneous system, show that the slower the B850 → B800 energy transfer, (i) the larger the differences between the fluorescence spectra upon B850 and B880 excitation at a given redox condition, and (ii) the larger the differences between the fluorescence spectra upon B880 excitation under different redox conditions.

All the experimental fluorescence spectra (Figs. 3–9) share the common feature that F_o and F_m conditions yield indistinguishable fluorescence spectra upon 900 nm excitation within the scatter of the data. This is only compatible with a fast B850 → B880 energy transfer of $\tau_{B850\rightarrow B880} \leq 5$ ps. As our theoretical simulations demonstrate, a $\tau_{B850\rightarrow B880} \leq 5$ ps energy transfer at either redox state predicts *small deviations in the fluorescence spectra depending on B850 or B880 excitation* (compare Fig. 10e and f). Such small deviations are experimentally found in *Rps. acidophila* (grown under high light), *Rps. palustris*, and *C. vinosum* but not in *Rps. acidophila* (LL and LL/LT), *Rb. sphaeroides*, and *C. purpuratum*. Therefore, it must be proposed that the latter species contain a small fraction of unconnected or poorly connected peripheral LH2 complexes and that the real system is not perfectly homogeneous. These are traceable in time-resolved measurements as long lived fluorescence decay phases with small or very small amplitudes as discussed by Sundström and van Grondelle [49]. Note that in the 900 nm excitation these unconnected LH2 rings are not excited and therefore do not contribute to the fluorescence spectrum. Additionally, these mal-connected LH2 rings only contribute to less than about 2% to the total absorption spectrum.

4.3.4. Further interpretation of the experimental data

The spectral decomposition of the photosynthetic unit in the different species of LH2+LH1 purple bacteria allows the calculation of the effective number of antenna pigments per RC N_{eff}, i.e. the sum over states, from the numbers tabulated in Table 2. This quantity describes the hypothetical antenna size if all antenna pigments were isoenergetic and is a determining factor for the overall fluorescence decay time [33]. It turns out that for all purple bacteria studied this is a rather invariant number of about 40 although the total number of BChl molecules varies by a factor of 2. In the idealized case of eight LH2 rings surrounding the core complex N_{eff} is slightly larger ($N_{eff} = 53$).

Using the values given in Table 2, it is also possible to calculate the equilibrium constants for the exciton exchange between the B850 and B880 pigments using the equation:

$$K = \frac{N_{B880}}{N_{B850}} e^{-\frac{E_{B880} - E_{B850}}{k_B T}} \quad (8)$$

All the calculated equilibrium constants ranged between 2 and 8 (Table 3). The fact that all constants were > 1 means that the equilibrium is on the B880 side and energy transfer generally occurs downhill.

In a recent paper by Law et al. [34] it was concluded from the deviation between the fluorescence spectra due to 802 nm and 896 nm excitation that the uphill energy transfer from B880 to B850 was unfavorable and represented a kinetic impediment. As shown by the above simulations this argument is not conclusive. Such a deviation may be caused either by the difference in the downhill versus uphill energy transfer kinetics or by a small fraction of unconnected or poorly connected peripheral LH2 complexes. The present data and their analysis show that in the majority of photosystems uphill energy transfer in LH2+LH1-containing purple bacteria occurs close to its thermodynamical maximal extent. Then the difference between the fluorescence spectra may also arise from loosely connected or unconnected light harvesting complexes.

Table 3
Total BChl antenna sizes, effective antenna sizes N_{eff} (sum over states) and thermodynamic equilibrium constants for exciton equilibration between B850 and B880 complexes calculated from the number of BChl molecules in each spectral pool and their absorption maxima according to the spectral decomposition (Table 2)

Species	N_{tot}	N_{eff}	K(B850 ↔ B880)
Hypothetical 8-ring case	248	53	1.55
Rps. acidophila	170	47	2.01
Rps. acidophila LL	193	43	3.02
Rps. acidophila LL/LT	194	37	9.7
Rps. palustris	91	42	3.30
Rb. sphaeroides 2.4.1	124	42	3.20
C. vinosum	91	41	3.11
C. purpuratum	244	39	4.50

In the case of *C. purpuratum* the equilibrium was calculated for the B830 ↔ B880 exciton transfer.

5. Summary and conclusions

The present work allows some general conclusions to be drawn about both the antenna organization and exciton dynamics in LH2+LH1-containing purple bacteria. These can be summarized as follows:

- In most purple bacteria the antenna size of the PSU seems to be smaller than that expected from the idealized model of the PSU in which each core complex is surrounded by eight LH2 rings.
- Thermodynamic equilibrium in the antenna system of these bacteria is a valid approximation for the interpretation of the stationary fluorescence spectra but only when the core complexes are excited.
- The transfer equilibrium does not deviate much from the thermodynamic equilibrium.
- The transfer equilibrium is established within a few picoseconds and not within a few tens of picoseconds.
- A small fraction of unconnected or loosely connected LH2 leads to excess fluorescence emission at around 830 nm which hampers the interpretation of the blue-excited (800 nm) fluorescence.

Acknowledgements

H.-W.T. thanks Prof. W. Junge for his general support and the laboratory facilities. The work was financially supported by the Deutsche Forschungsgemeinschaft (SFB 171-A1), the BBSRC (R.J.C), and the ESF (C.J.L).

Appendix

A.1. A two state reversible reaction scheme

Consider a reversible reaction between A and B with the rate constants k_1 and k_{-1}:

$$D \xleftarrow{k_\ell} A \underset{k_{-1}}{\overset{k_1}{\rightleftarrows}} B \xrightarrow{k_2} C$$

with the aim of collecting all conceivable solutions and the relations between them for the initial conditions $A(t=0)=1$ and $B(t=0)=1$.

A.2. Excitation in A

State A can decay with the rate constant k_ℓ into D and B with k_2 into C. The time dependence of the states are simple exponential functions, if the single initial state is $A(0)=1$ and $B(0)=C(0)=D(0)=0$:

$$A(t) = a_1 \cdot e^{-\gamma_1 \cdot t} + a_2 \cdot e^{-\gamma_2 \cdot t} \tag{A1a}$$

$$B(t) = \frac{k_1}{\gamma_1 - \gamma_2}(e^{-\gamma_2 \cdot t} - e^{-\gamma_1 \cdot t}) \tag{A1b}$$

$$C(t) = \frac{k_1 \cdot k_2}{\gamma_1 - \gamma_2}\left(\frac{1}{\gamma_1}e^{-\gamma_1 \cdot t} - \frac{1}{\gamma_2}e^{-\gamma_2 \cdot t} + \frac{\gamma_1 - \gamma_2}{\gamma_1 \cdot \gamma_2}\right) \tag{A1c}$$

$$D(t) = 1 - A(t) - B(t) - C(t) \tag{A1d}$$

with the amplitude factors:

$$a_1 = \frac{\gamma_1 - k_{-1} - k_2}{\gamma_1 - \gamma_2} \tag{A2a}$$

$$a_2 = \frac{\gamma_2 - k_{-1} - k_2}{\gamma_2 - \gamma_1} \tag{A2b}$$

and the apparent rate constants:

$$\gamma_1 = \frac{1}{2}[(k_\ell + k_1 + k_{-1} + k_2) + \sqrt{(k_\ell + k_1 - k_{-1} - k_2)^2 + 4k_1 k_{-1}}] \tag{A2c}$$

$$\gamma_2 = \tfrac{1}{2}[(k_\ell + k_1 + k_{-1} + k_2) - \sqrt{(k_\ell + k_1 - k_{-1} - k_2)^2 + 4k_1 k_{-1}}] \tag{A2d}$$

It is worth mentioning that there exists a simple identity between the molecular and the apparent rate constants which reads:

$$\frac{k_1}{\gamma_{1,2} - k_\ell} + \frac{k_{-1}}{\gamma_{1,2} - k_2} \equiv 1 \tag{A3}$$

It is clear that A and B are only transiently formed whereas C and D adopt final values for $t \to \infty$. The yields of A and B are given by the time integrals of $A(t)$ and $B(t)$:

$$\Phi_A = \int_0^\infty A(t)\mathrm{d}t = \frac{a_1}{\gamma_1} + \frac{a_2}{\gamma_2} \tag{A4a}$$

$$\Phi_B = \int_0^\infty B(t)\mathrm{d}t = \frac{k_1}{\gamma_1 \cdot \gamma_2} \tag{A4b}$$

whereas the quantum yields of C and D follow from their infinite values:

$$\Phi_C = \lim_{t\to\infty} C(t) = \frac{k_1 \cdot k_2}{\gamma_1 \cdot \gamma_2} \tag{A4c}$$

$$\Phi_D = \lim_{t\to\infty} D(t) = 1 - \frac{k_1 \cdot k_2}{\gamma_1 \cdot \gamma_2} \tag{A4d}$$

Another useful quantity is the ratio of the yields of the transient states A and B:

$$\frac{\Phi_B}{\Phi_A} = \frac{k_1}{a_1 \cdot \gamma_2 + a_2 \cdot \gamma_1} = \frac{k_1}{k_{-1} + k_2} \tag{A5}$$

After the initiation of the reaction the transient states $A(t)$ and $B(t)$ will reach an equilibrium state in which the decay occurs with the same kinetics. The equilibration kinetics is given by the ratio of $B(t)$ and $A(t)$ according to:

$$\tilde{K}(t) = \frac{B(t)}{A(t)} \tag{A6a}$$

The limiting value of this quantity, which is the transfer equilibrium, is easily obtained for $t \to \infty$:

$$\tilde{K}^0 = \lim_{t\to\infty} \tilde{K}(t) = \frac{k_1}{a_2(\gamma_1 - \gamma_2)} \tag{A6b}$$

Depending on the rate constants this transfer equilibrium constant $\tilde{K}^0$ may significantly deviate from the thermodynamic equilibrium constant, $K = k_1/k_{-1}$ (see Fig. 10b).

A.3. Excitation in B

The solutions, if the initial state is $B(0) = 1$ and $A(0) = C(0) = D(0) = 0$, have the same analytical form and can be obtained for symmetry reasons by replacing $A \to B$, $B \to A$, $C \to D$, $D \to C$, $k_\ell \to k_2$, $k_1 \to k_{-1}$, $k_2 \to k_\ell$, $k_{-1} \to k_1$. The amplitude factors and the apparent rate constants (Eqs. A2a–A2d) remain the same. Using the above substitutions we obtain for the time-dependent states:

$$A(t) = \frac{k_{-1}}{\gamma_1 - \gamma_2}(e^{-\gamma_2 \cdot t} - e^{-\gamma_1 \cdot t}) \tag{A7a}$$

$$B(t) = a_1 \cdot e^{-\gamma_2 \cdot t} + a_2 \cdot e^{-\gamma_1 \cdot t} \tag{A7b}$$

$$D(t) = \frac{k_{-1} \cdot k_\ell}{\gamma_1 - \gamma_2}\left(\frac{1}{\gamma_1} e^{-\gamma_1 \cdot t} - \frac{1}{\gamma_2} e^{-\gamma_2 \cdot t} + \frac{\gamma_1 - \gamma_2}{\gamma_1 \cdot \gamma_2}\right) \tag{A7c}$$

$$C(t) = 1 - A(t) - B(t) - D(t) \tag{A7d}$$

The identity equation (Eq. A3) remains preserved.

As before, the yields of A and B are given by the time integrals of $A(t)$ and $B(t)$:

$$\Phi_A = \int_0^\infty A(t)\mathrm{d}t = \frac{k_{-1}}{\gamma_1 \cdot \gamma_2} \tag{A8a}$$

$$\Phi_B = \int_0^\infty B(t)\mathrm{d}t = \frac{a_1}{\gamma_2} + \frac{a_2}{\gamma_1} \tag{A8b}$$

whereas the quantum yields of C and D follow from their infinite values:

$$\Phi_C = \lim_{t\to\infty} C(t) = 1 - \frac{k_{-1} \cdot k_\ell}{\gamma_1 \cdot \gamma_2} \tag{A8c}$$

$$\Phi_D = \lim_{t\to\infty} D(t) = \frac{k_{-1} \cdot k_\ell}{\gamma_1 \cdot \gamma_2} \tag{A8d}$$

The ratio of the yields of the transient states A and B is given by:

$$\frac{\Phi_B}{\Phi_A} = \frac{a_1 \cdot \gamma_1 + a_2 \cdot \gamma_2}{k_{-1}} = \frac{k_1 + k_\ell}{k_{-1}} \tag{9}$$

For completeness, it should be mentioned that the transfer equilibrium (Eq. 6a) is independent of the type of excitation and is therefore the same.

References

[1] R.T. Wang, J. Myers, Plant Cell Physiol. Special Issue (1977) 3–7.
[2] A. Sonneveld, H. Rademaker, L.N.M. Duysens, FEBS Lett. 113 (1980) 323–327.
[3] S.W. McCauley, E. Bittersmann, A.R. Holzwarth, FEBS Lett. 249 (1989) 285–288.
[4] K.L. Zankel, R.K. Clayton, Photochem. Photobiol. 9 (1969) 7–15.
[5] M.Z. Papiz, S.M. Prince, A.M. Hawthornthwaite, G. McDermott, A.A. Freer, N.W. Isaacs, R.J. Cogdell, Trends Plant Sci. 1 (1996) 198–206.
[6] H.M. Visser, O.J.G. Somsen, F. van Mourik, S. Lin, I.H.M. van Stokkum, R. van Grondelle, Biophys. J. 69 (1995) 1083–1099.

[7] G. McDermott, S.M. Prince, A.A. Freer, A.M. Hawthornthwaite, M.Z. Papiz, R.J. Cogdell, N.W. Isaacs, Nature 374 (1995) 517–521.
[8] J. Koepke, X.C. Hu, C. Muenke, K. Schulten, H. Michel, Structure 4 (1996) 581–597.
[9] H. Zuber, R.J. Cogdell, in: R.E. Blankenship, M.T. Madigan, C.E. Bauer (Eds.), Anoxygenic Photosythetic Bacteria, Kluwer Academic Publishers, Dordrecht, 1995, pp. 315–348.
[10] S. Karrasch, P.A. Bullough, R. Ghosh, EMBO J. 14 (1995) 631–638.
[11] R. van Grondelle, Biochim. Biophys. Acta 811 (1985) 147–195.
[12] M.G. Müller, G. Drews, A.R. Holzwarth, Biochim. Biophys. Acta 1142 (1993) 49–58.
[13] K. Shimada, M. Mimuro, N. Tamai, I. Yamazaki, Biochim. Biophys. Acta 975 (1989) 72–79.
[14] V. Sundström, R. van Grondelle, H. Bergström, E. Akesson, T. Gillbro, Biochim. Biophys. Acta 851 (1986) 431–446.
[15] P.D. Laible, W. Zipfel, T.G. Owens, Biophys. J. 66 (1994) 844–860.
[16] S. Hess, M. Chachisvilis, K. Timpmann, M.R. Jones, G.J.S. Fowler, C.N. Hunter, V. Sundström, Proc. Natl. Acad. Sci. USA 92 (1995) 12333–12337.
[17] S. Hess, E. Akesson, R.J. Cogdell, T. Pullerits, V. Sundström, Biophys. J. 69 (1995) 2211–2225.
[18] A.P. Shreve, J.K. Trautman, H.A. Frank, T.G. Owens, A.C. Albrecht, Biochim. Biophys. Acta 1058 (1991) 280–288.
[19] H. Bergström, V. Sundström, R. van Grondelle, T. Gillbro, R.J. Cogdell, Biochim. Biophys. Acta 936 (1988) 90–98.
[20] J.T.M. Kennis, A.M. Streltsov, T.J. Aartsma, T. Nozawa, J. Amesz, J. Phys. Chem. B 100 (1996) 2438–2442.
[21] S. Hess, F. Feldchtein, A. Babin, I. Nurgaleev, T. Pullerits, A. Sergeev, Chem. Phys. Lett. 216 (1993) 247–257.
[22] R. Monshouwer, I.O. de Zarate, F. van Mourik, R. van Grondelle, Chem. Phys. Lett. 246 (1995) 341–346.
[23] R. van Grondelle, H.J.M. Kramer, C.P. Rijgersberg, Biochim. Biophys. Acta 682 (1982) 208–215.
[24] V. Nagarajan, W.W. Parson, Biochemistry 36 (1997) 2300–2306.
[25] F.G. Zhang, R. van Grondelle, V. Sundström, Biophys. J. 61 (1992) 911–920.
[26] J.T.M. Kennis, T.J. Aartsma, J. Amesz, Chem. Phys. 194 (1995) 285–289.
[27] S. Hess, K. Visscher, J. Ulander, T. Pullerits, M.R. Jones, C.N. Hunter, V. Sundström, Biochemistry 32 (1993) 10314–10322.
[28] L.M.P. Beekman, F. van Mourik, M.R. Jones, H.M. Visser, C.N. Hunter, R. van Grondelle, Biochemistry 33 (1994) 3143–3147.
[29] J.T.M. Kennis, T.J. Aartsma, J. Amesz, Biochim. Biophys. Acta 1188 (1994) 278–286.
[30] A.P. Razjivin, R.V. Danielius, R.A. Gadonas, A.Y. Borisov, A.S. Piskarskas, FEBS Lett. 143 (1982) 40–44.
[31] T.G. Monger, R.J. Cogdell, W.W. Parson, Biochim. Biophys. Acta 449 (1976) 136–153.
[32] K. Timpmann, F.G. Zhang, A. Freiberg, V. Sundström, Biochim. Biophys. Acta 1183 (1993) 185–193.
[33] H.-W. Trissl, Photosynth. Res. 35 (1993) 247–263.
[34] C.J. Law, R.J. Cogdell, H.-W. Trissl, Photosynth. Res. 52 (1997) 157–165.
[35] A.M. Hawthornthwaite, R.J. Cogdell, in: H. Scheer (Ed.), Chlorophylls, CRC Press, Boca Raton, FL, 1991, pp. 493–528.
[36] X. Hu, T. Ritz, A. Damjanovic, K. Schulten, J. Phys. Chem. B 101 (1997) 3854–3871.
[37] R.J. Cogdell, N.W. Isaacs, A.A. Freer, J. Arrelano, T.D. Howard, M.Z. Papiz, A.M. Hawthornthwaitelawless, S. Prince, Prog. Biophys. Mol. Biol. 68 (1997) 1–27.
[38] H.-W. Trissl, C.J. Law, R.J. Cogdell, in: G. Garab, J. Pusztai (Eds.), Proceedings of the XIth International Congress on Photosynthesis, 1998, Vol. 1, Kluwer Academic Publishers, The Netherlands, pp. 65–68.
[39] R.C. Jennings, G. Zucchelli, R. Croce, L. Valkunas, L. Finzi, F.M. Garlaschi, Photosynth. Res. 52 (1997) 245–253.
[40] R. Croce, G. Zucchelli, F.M. Garlaschi, R. Bassi, R.C. Jennings, Biochemistry 35 (1996) 8572–8579.
[41] H. Dau, K. Sauer, Biochim. Biophys. Acta 1273 (1996) 175–190.
[42] G. Zucchelli, F.M. Garlaschi, R. Croce, R. Bassi, R.C. Jennings, Biochim. Biophys. Acta 1229 (1995) 59–63.
[43] H. Dau, Photosynth. Res. 48 (1996) 139–145.
[44] B.I. Stepanov, Sov. Phys. Dokl. 2 (1957) 81–84.
[45] E.H. Kennard, Phys. Rev. 11 (1918) 29–38.
[46] M.A. Bopp, Y.W. Jia, L.Q. Li, R.J. Cogdell, R.M. Hochstrasser, Proc. Natl. Acad. Sci. USA 94 (1997) 10630–10635.
[47] R. Jiminez, S.N. Dikshit, S.E. Bradforth, G.R. Fleming, J. Phys. Chem. 100 (1996) 6825–6834.
[48] S.E. Bradforth, R. Jiminez, F. van Mourik, R. van Grondelle, G.R. Fleming, J. Phys. Chem. B 99 (1995) 16179–16191.
[49] V. Sundström, R. van Grondelle, in: R.E. Blankenship, M.T. Madigan, C.E. Bauer (Eds.), Anoxygenic Photosynthetic Bacteria, Kluwer Academic Publishers, Dordrecht, 1995, pp. 349–372.
[50] G.R. Fleming, R. van Grondelle, Curr. Opin. Struct. Biol. 7 (1997) 738–748.
[51] R. van Grondelle, J.P. Dekker, T. Gillbro, V. Sundström, Biochim. Biophys. Acta 1187 (1994) 1–65.
[52] C.A. Kerfeld, T.O. Yeates, J.P. Thornber, Biochemistry 33 (1994) 2178–2184.
[53] C. Francke, J. Amesz, Photosynth. Res. 46 (1995) 347–352.
[54] P. McGlynn, W.H.J. Westerhuis, M.R. Jones, C.N. Hunter, J. Biol. Chem. 271 (1996) 3285–3292.
[55] R.J. Pugh, P. McGlynn, M.R. Jones, C.N. Hunter, Biochim. Biophys. Acta 1366 (1998) 301–316.
[56] H. Kramer, C. Francke, C.N. Hunter, J. Amesz, in: G. Garab, J. Pusztai (Eds.), Proceedings of the XIth International Congress on Photosynthesis, 1998, Vol. 1, Kluwer Academic Publishers, The Netherlands, pp. 89–92.

[57] K. Sauer, R.J. Cogdell, S.M. Prince, A. Freer, N.W. Isaacs, H. Scheer, Photochem. Photobiol. 64 (1996) 564–576.
[58] R. Monshouwer, R. van Grondelle, Biochim. Biophys. Acta 1275 (1996) 70–75.
[59] X. Hu, K. Schulten, Biophys. J. 75 (1998) 683–694.
[60] R. Monshouwer, M. Abrahamsson, F. van Mourik, R. van Grondelle, J. Phys. Chem. B 101 (1997) 7241–7248.
[61] W. Zinth, P. Huppmann, T. Arlt, J. Wachtveitl, Phil. Trans. R. Soc. London Biol. 356 (1998) 465–476.